

First lattice calculation of radiative leptonic decay rates of pseudoscalar mesons

A. Desiderio,¹ R. Frezzotti,¹ M. Garofalo,² D. Giusti,^{3,4} M. Hansen,⁵ V. Lubicz,²
G. Martinelli,⁶ C.T. Sachrajda,⁷ F. Sanfilippo,⁴ S. Simula,⁴ and N. Tantalo¹

¹*Dipartimento di Fisica and INFN, Università di Roma “Tor Vergata”, Via della Ricerca Scientifica 1, I-00133 Roma, Italy*

²*Dipartimento di Fisica, Università Roma Tre and INFN, Sezione di Roma Tre, Via della Vasca Navale 84, I-00146 Rome, Italy*

³*Universität Regensburg, Fakultät für Physik, Universitätsstrasse 31, 93040 Regensburg, Germany*

⁴*Istituto Nazionale di Fisica Nucleare, Sezione di Roma Tre, Via della Vasca Navale 84, I-00146 Rome, Italy*

⁵*SDU eScience Center, University of Southern Denmark, Campusvej 55, DK-5230 Odense M, Denmark*

⁶*Physics Department and INFN Sezione di Roma La Sapienza Piazzale Aldo Moro 5, 00185 Roma, Italy*

⁷*Department of Physics and Astronomy, University of Southampton, Southampton SO17 1BJ, UK*

We present a non-perturbative lattice calculation of the form factors which contribute to the amplitudes for the radiative decays $P \rightarrow \ell \bar{\nu}_\ell \gamma$, where P is a pseudoscalar meson and ℓ is a charged lepton. Together with the non-perturbative determination of the corrections to the processes $P \rightarrow \ell \bar{\nu}_\ell$ due to the exchange of a virtual photon, this allows accurate predictions at $O(\alpha_{em})$ to be made for leptonic decay rates for pseudoscalar mesons ranging from the pion to the D_s meson. We are able to separate unambiguously and non-perturbatively the point-like contribution, from the structure-dependent, infrared-safe, terms in the amplitude. The fully non-perturbative $O(a)$ improved calculation of the inclusive leptonic decay rates will lead to the determination of the corresponding Cabibbo-Kobayashi-Maskawa (CKM) matrix elements also at $O(\alpha_{em})$. Prospects for a precise evaluation of leptonic decay rates with emission of a hard photon are also very interesting, especially for the decays of heavy D and B mesons for which currently only model-dependent predictions are available to compare with existing experimental data.

I. INTRODUCTION

The unitarity of the CKM matrix is one of the most precise tests of the Standard Model. Indeed, CKM unitarity may rule out many theoretically well motivated models for new physics and put severe constraints on the energy scale where new phenomena might occur, well beyond the range accessible to direct experimental searches. In this respect, leptonic decay rates of light and heavy pseudoscalar mesons are essential ingredients for the extraction of the CKM matrix elements. A first-principles calculation of these quantities requires non-perturbative accuracy and hence numerical lattice simulations. Moreover, in order to fully exploit the presently available experimental information and to perform the next generation of flavour-physics tests, $O(\alpha_{em})$ electromagnetic corrections must be included. In this endeavour, the radiative leptonic decays $P \rightarrow \ell \bar{\nu}_\ell(\gamma)$ (where P is a negatively charged pseudoscalar meson, ℓ a lepton, $\bar{\nu}_\ell$ the corresponding anti-neutrino and γ a photon) are particularly important, see [1].

Knowledge of the radiative leptonic decay rate in the region of small (soft) photon energies is required in order to properly define the infrared-safe measurable decay rate for the process $P \rightarrow \ell \bar{\nu}_\ell(\gamma)$. Indeed, according to the well-known Bloch-Nordsieck mechanism [2], the integral of the radiative decay rate in the phase space region corresponding to soft photons must be added to the decay rate with no real photons in the final states (the so-called virtual rate) in order to cancel infrared divergent contributions appearing in unphysical quantities at intermediate stages of the calculations.

On the one hand, in the limit of ultra-soft photon energy the radiative decay rate can be reliably calculated in an effective theory in which the meson is treated as a point-like particle. This is a manifestation of the well-known mechanism known as the “universality of infrared divergences” (see for example Ref. [3, 4]) that finds its physical explanation in the fact that ultra-soft photons cannot resolve the internal structure of the meson. On the other hand, the ultra-soft limit is an idealisation and experimental measurements, particularly in the case of heavy mesons, are inclusive up to photon energies that may be too large to safely neglect the Structure-Dependent (SD) corrections to the point-like approximation.

In the region of hard (experimentally detectable) photon energies, radiative leptonic decays represent important probes of the internal structure of the mesons. Moreover, radiative decays can provide independent determinations of CKM matrix elements with respect to the purely leptonic channels. A non-perturbative calculation of the radiative decay rates can be particularly important for heavy mesons since, unlike the case of pions and kaons where such decays have been studied

using Chiral Perturbation Theory (ChPT) [5–9], no model-independent calculations have ever been performed. Even in the case of light mesons, although the quoted ChPT calculations represent a first-principles approach to the problem, the low-energy constants entering in the final results at $O(p^6)$ have been estimated in phenomenological analyses relying in part on model-dependent assumptions.

In Ref. [10] a strategy to compute QED radiative corrections to the $P \rightarrow \ell \bar{\nu}_\ell(\gamma)$ decay rates at $O(\alpha_{em})$ by starting from first-principles lattice calculations was proposed. The strategy has subsequently been applied in Refs. [11–15], within the RM123 approach [16, 17], to provide the first non-perturbative model-independent calculation of the decay rates $\pi^- \rightarrow \mu^- \bar{\nu}_\mu(\gamma)$ and $K^- \rightarrow \mu^- \bar{\nu}_\mu(\gamma)$. In these calculations the real soft-photon contributions have been evaluated in the point-like effective theory and, using the ChPT results quoted above, the SD corrections have been estimated to be negligible for these processes (see [10]). In the same phenomenological analysis it has been shown that the SD corrections might instead be relevant for the decays of pions and kaons into electrons. Moreover, by using the same single-pole dominance approximation as originally used in Ref. [18], SD contributions have been estimated to be phenomenologically important for decays of heavy-flavour mesons.

In this paper we present the first non-perturbative lattice calculation of the rates for the radiative decays $P \rightarrow \ell \bar{\nu} \gamma$, where P is a pion, kaon, D or D_s meson. We use the $N_f = 2 + 1 + 1$ gauge ensembles generated by the European Twisted Mass Collaboration (ETMC) and analysed for mesonic observables in Ref. [19]. Preliminary results from this study were presented in Ref. [20]; the decays of bottom mesons will be studied in future papers. Note also that Kane et al. have presented preliminary results for the decays $D_s^+ \rightarrow \ell^+ \nu \gamma$ and $K^- \rightarrow \ell^- \bar{\nu} \gamma$, where ℓ^\pm represents the charged leptons and γ is a hard photon with energy in the range of about 0.5-1 GeV in Ref. [21].

The plan of the remainder of this paper is as follows. In Section II we introduce the basic quantities which enter in the amplitude for the leptonic decay of a pseudoscalar meson with the emission of a real photon; in particular we define the axial and vector form factors F_A and F_V . We express the decay rates in terms of these quantities in Appendix A. In Section III we describe the general strategy that we followed to extract the amplitudes from suitable Euclidean correlation functions and discuss finite-time effects. The presence of discretisation effects which diverge at small photon momenta is demonstrated in Section IV and Appendix C, together with a strategy for subtracting them non-perturbatively. In Section V we present the numerical results for pions, kaons, D and D_s mesons. Many formulae which are used in the paper are discussed and derived in Appendices A-C. Finally, in Appendix D we present some of our numerical results, including the

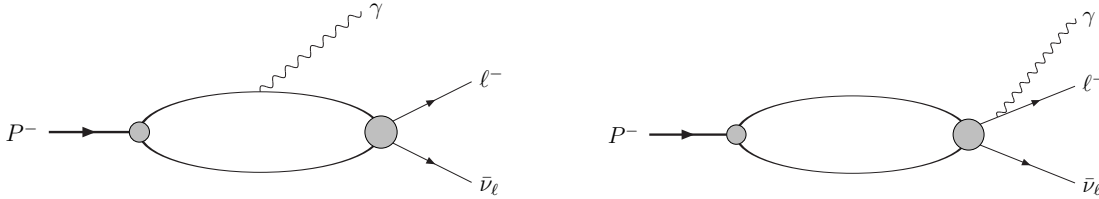


FIG. 1: Feynman diagrams representing the amplitudes with the emission of a real photon from the P^- meson (left panel) or from the final-state charged lepton ℓ^- (right panel).

correlation matrices, in a way which we hope may be useful to readers who wish to use them in phenomenological applications.

II. DEFINITION OF THE FORM FACTORS

The non-perturbative contribution to the radiative leptonic decay rate for the processes $P \rightarrow \ell \bar{\nu}_\ell \gamma$ is encoded in the following hadronic matrix-element, see left panel of Fig. 1,

$$H_W^{\alpha r}(k, \mathbf{p}) = \epsilon_\mu^r(k) H_W^{\alpha\mu}(k, \mathbf{p}) = \epsilon_\mu^r(k) \int d^4y e^{ik \cdot y} \mathbb{T} \langle 0 | j_W^\alpha(0) j_{em}^\mu(y) | P(\mathbf{p}) \rangle, \quad (1)$$

where $\epsilon_\mu^r(k)$ is the polarisation vector of the outgoing photon with four-momentum k , \mathbf{p} is the momentum of the ingoing pseudoscalar meson of mass m_P ($p \equiv (E, \mathbf{p})$, $E = \sqrt{m_P^2 + \mathbf{p}^2}$ and $p^2 = m_P^2$). The operators

$$j_{em}^\mu(x) = \sum_f q_f \bar{\psi}_f(x) \gamma^\mu \psi_f(x), \quad j_W^\alpha(x) = j_V^\alpha(x) - j_A^\alpha(x) = \bar{\psi}_U(x) (\gamma^\alpha - \gamma^\alpha \gamma_5) \psi_D(x), \quad (2)$$

are respectively the electromagnetic hadronic current and the hadronic weak current expressed in terms of the quark fields ψ_f having electric charge q_f in units of the charge of the positron; ψ_U and ψ_D indicate the fields of an up-type or a down-type quark and for the mesons considered in this study U can be either an up or a charm quark and D a down or a strange quark. In order to calculate the full amplitude one has also to consider the contribution in which the photon is emitted from the final-state charged lepton, see the right panel of Fig. 1. This latter contribution however, can be computed in perturbation theory using the meson's decay constant f_P . Both contributions are included in the formulae for the decay rate given in appendix A.

The decomposition of $H_W^{\alpha r}(k, \mathbf{p})$ in terms of scalar form factors has been discussed in Ref. [10]

(see also [22]). Here we adopt the same basis used in that paper to write

$$\begin{aligned}
H_W^{\alpha r}(k, \mathbf{p}) = \epsilon_\mu^r(k) & \left\{ H_1 [k^2 g^{\mu\alpha} - k^\mu k^\alpha] + H_2 [(p \cdot k - k^2)k^\mu - k^2(p - k)^\mu] (p - k)^\alpha \right. \\
& - i \frac{F_V}{m_P} \varepsilon^{\mu\alpha\gamma\beta} k_\gamma p_\beta + \frac{F_A}{m_P} [(p \cdot k - k^2)g^{\mu\alpha} - (p - k)^\mu k^\alpha] \\
& \left. + f_P \left[g^{\mu\alpha} + \frac{(2p - k)^\mu (p - k)^\alpha}{2p \cdot k - k^2} \right] \right\}. \tag{3}
\end{aligned}$$

The term in the last line of Eq. (3), which we write as $H_{pt}^{\alpha\mu}(k, \mathbf{p})$, is the point-like infrared-divergent contribution. The other terms correspond to the so called SD contribution, $H_{SD}^{\alpha\mu}(k, \mathbf{p})$. $H_{pt}^{\alpha\mu}(k, \mathbf{p})$ saturates the Ward Identity (WI) satisfied by $H_W^{\alpha\mu}(k, \mathbf{p})$

$$k_\mu H_W^{\alpha\mu}(k, \mathbf{p}) = k_\mu H_{pt}^{\alpha\mu}(k, \mathbf{p}) = i \langle 0 | j_W^\alpha(0) | P(\mathbf{p}) \rangle = f_P p^\alpha, \quad k_\mu H_{SD}^{\alpha\mu}(k, \mathbf{p}) = 0, \tag{4}$$

as explained in detail in Appendix C. The four form factors $H_{1,2}$ and $F_{V,A}$ are scalar functions of Lorentz invariants, m_P^2 , $p \cdot k$ and k^2 . Eq. (3) is valid for generic (off-shell) values of the photon momentum and for generic choices of the polarisation vectors. The knowledge of the four form factors in the case of off-shell photons ($k^2 \neq 0$) gives access to the study of decays in which the pseudoscalar meson decays into four leptons. These processes are very interesting in the search of physics beyond the Standard Model and will be the subject of a future work. In this paper we concentrate on the case in which the photon is on-shell.

By setting $k^2 = 0$, at fixed meson mass, the form factors are functions of $p \cdot k$ only. Moreover, by choosing a *physical* basis for the polarisation vectors so that

$$\epsilon_r(\mathbf{k}) \cdot k = 0, \tag{5}$$

one has

$$H_W^{\alpha r}(k, \mathbf{p}) = \epsilon_\mu^r(\mathbf{k}) \left\{ -i \frac{F_V}{m_P} \varepsilon^{\mu\alpha\gamma\beta} k_\gamma p_\beta + \left[\frac{F_A}{m_P} + \frac{f_P}{p \cdot k} \right] (p \cdot k g^{\mu\alpha} - p^\mu k^\alpha) + \frac{f_P}{p \cdot k} p^\mu p^\alpha \right\}. \tag{6}$$

Once the decay constant f_P and the two SD axial and vector form factors F_A and F_V are known, the radiative decay rate can be calculated by using the formulae given in appendix A. These formulae are expressed in terms of the convenient dimensionless variable

$$x_\gamma = \frac{2p \cdot k}{m_P^2} \quad \text{with} \quad 0 \leq x_\gamma \leq 1 - \frac{m_\ell^2}{m_P^2}, \tag{7}$$

where m_ℓ is the mass of the outgoing lepton in the $P \rightarrow \ell \bar{\nu}_\ell \gamma$ decay.

Our definition of the form factor F_A differs from the definition, F_A^B , of refs. [21, 23]

$$F_A^B = F_A + \frac{m_P f_P}{p \cdot k}. \quad (8)$$

We note that F_A^B includes the point-like infrared divergent contribution which totally dominates at low values of x_γ thus obscuring the interesting structure-dependent contribution. For this reason we strongly advocate the use of our definition [10]. Moreover the sign of F_V used in this paper is opposite to the one used in Ref. [21].

III. FORM FACTORS FROM EUCLIDEAN CORRELATION FUNCTIONS

In order to relate the hadronic matrix element to Euclidean correlation functions, the primary quantities computed in lattice calculations, it is useful to express the $H_W^{\alpha r}(k, \mathbf{p})$, defined in Eq. (1) in Minkowski space in terms of the contributions coming from the different time orderings. To this end, we define

$$H_W^{\alpha r}(k, \mathbf{p}) = H_{W,1}^{\alpha r}(k, \mathbf{p}) + H_{W,2}^{\alpha r}(k, \mathbf{p}), \quad j^r(\mathbf{k}) = \epsilon_\mu^r(\mathbf{k}) \int d^3 y e^{-i\mathbf{k}\cdot\mathbf{y}} j_{em}^\mu(0, \mathbf{y}), \quad (9)$$

and perform the t_y integral,

$$\begin{aligned} H_{W,1}^{\alpha r}(k, \mathbf{p}) &= \int_{-\infty}^0 dt_y e^{iE_\gamma t_y} \langle 0 | j_W^\alpha(0) e^{i(\hat{H}-E-i\varepsilon)t_y} j^r(\mathbf{k}) | P(\mathbf{p}) \rangle \\ &= -i \langle 0 | j_W^\alpha(0) \frac{1}{\hat{H} + E_\gamma - E - i\varepsilon} j^r(\mathbf{k}) | P(\mathbf{p}) \rangle, \\ H_{W,2}^{\alpha r}(k, \mathbf{p}) &= \int_0^\infty dt_y e^{iE_\gamma t_y} \langle 0 | j^r(\mathbf{k}) e^{-i(\hat{H}-i\varepsilon)t_y} j_W^\alpha(0) | P(\mathbf{p}) \rangle \\ &= -i \langle 0 | j^r(\mathbf{k}) \frac{1}{\hat{H} - E_\gamma - i\varepsilon} j_W^\alpha(0) | P(\mathbf{p}) \rangle, \end{aligned} \quad (10)$$

where \hat{H} is the QCD Hamiltonian operator, $E = \sqrt{m_P^2 + \mathbf{p}^2}$ is the energy of the decaying meson P and $E_\gamma = |\mathbf{k}|$ is the energy of the outgoing real photon.

The important observation that makes the lattice calculation possible by using standard effective-mass/residue techniques is that the integrals over t_y appearing in the definition of $H_W^{\alpha r}(k, \mathbf{p})$ can be Wick rotated to the Euclidean space without encountering any obstruction. Such obstructions arise whenever there are states propagating between the operators in the T-products that have energies smaller than the energy of the external states [24]. This doesn't

happen in our case. For this reason $H_{W,1,2}^{\alpha r}(k, \mathbf{p})$ can be rewritten in terms of Euclidean integrals,

$$H_{W,1}^{\alpha r}(k, \mathbf{p}) = -i \int_{-\infty}^0 dt_y \langle 0 | j_W^\alpha(0) e^{(\hat{H} + E_\gamma - E)t_y} j^r(\mathbf{k}) | P(\mathbf{p}) \rangle$$

$$H_{W,2}^{\alpha r}(k, \mathbf{p}) = -i \int_0^\infty dt_y \langle 0 | j^r(\mathbf{k}) e^{-(\hat{H} - E_\gamma)t_y} j_W^\alpha(0) | P(\mathbf{p}) \rangle, \quad (11)$$

both of which are convergent for physical (non-vanishing) photon energies. In Eqs. (11) and below t_y is a Euclidean time variable. Indeed, the hadronic state of lowest energy that can propagate between the two currents is the pseudoscalar meson with spatial momentum $\mathbf{p} - \mathbf{k}$ (it appears in the time-ordering $H_{W,1}^{\alpha r}$) and we have

$$\sqrt{m_P^2 + (\mathbf{p} - \mathbf{k})^2} + E_\gamma > \sqrt{m_P^2 + \mathbf{p}^2}, \quad |\mathbf{k}| \neq 0. \quad (12)$$

As a consequence, $H_W^{\alpha r}(k, \mathbf{p})$ can be rewritten as

$$H_W^{\alpha r}(k, \mathbf{p}) = -i \int d^4y e^{E_\gamma t_y - i\mathbf{k} \cdot \mathbf{y}} \epsilon_\mu^r(\mathbf{k}) \text{T} \langle 0 | j_W^\alpha(0) j_{em}^\mu(y) | P(\mathbf{p}) \rangle. \quad (13)$$

From this observation it follows that the hadronic matrix-element can be extracted from the Euclidean correlation functions

$$C_W^{\alpha r}(t; \mathbf{k}, \mathbf{p}) = -i \epsilon_\mu^r(\mathbf{k}) \int d^4y d^3\mathbf{x} e^{t_y E_\gamma - i\mathbf{k} \cdot \mathbf{y} + i\mathbf{p} \cdot \mathbf{x}} \text{T} \langle 0 | j_W^\alpha(t) j_{em}^\mu(y) P(0, \mathbf{x}) | 0 \rangle, \quad (14)$$

where $P = i\bar{\psi}_D \gamma_5 \psi_U$ is a Hermitian pseudoscalar interpolating operator having the flavour quantum numbers of the incoming meson. In Eq. (14), using the translational invariance of the correlation function, we have moved the origin in time to the pseudoscalar source, $P(0, \mathbf{x})$, and placed the weak current at t .

In the large- t limit one has

$$R_W^{\alpha r}(t; \mathbf{k}, \mathbf{p}) = \frac{2E}{e^{-t(E-E_\gamma)} \langle P(\mathbf{p}) | P(0) | 0 \rangle} C_W^{\alpha r}(t; \mathbf{k}, \mathbf{p}) = H_W^{\alpha r}(k, \mathbf{p}) + \dots \quad (15)$$

where the ellipsis represents the sub-leading exponentials.

The expressions for the correlation function $C_W^{\alpha r}(t; \mathbf{k}, \mathbf{p})$ in Eq. (14) and for the ratio $R_W^{\alpha r}(t; \mathbf{k}, \mathbf{p})$ in Eq. (15) refer to the ideal case of a lattice with infinite time-extent. The extraction of the matrix elements from correlation functions computed on a finite lattice in our numerical simulations is discussed in Appendix B. Although some of the details of the appendix refer to our specific lattice procedures (the choice of lattice Fermions, renormalisation of the operators, etc.) the strategy itself is general and can be directly translated to other lattice discretisations of QCD and of QED.

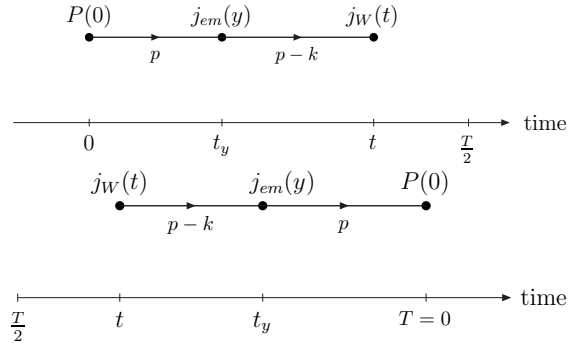


FIG. 2: Schematic diagrams representing the correlation function $C_W^{\alpha r}(t, T/2; \mathbf{k}, \mathbf{p})$ used to extract the form factors, see Appendix B. The interpolating operator for the meson P and the weak current j_W are placed at fixed times 0 and t , and the electromagnetic current j_{em} is inserted at t_y which is integrated over $0 \leq t_y \leq T$, where T is the temporal extent of the lattice. The left and right panels correspond to the leading contributions to the correlation functions for $t_y < T/2$ and $t_y > T/2$ respectively, with mesons propagating with momenta p or $p - k$.

Here in the main text, we use Fig. 2 to illustrate the strategy used in our numerical simulations, performed with (anti-) periodic boundary conditions in time for the (fermionic) bosonic fields, to extract the form factors. The two panels in Fig. 2 represent the *forward* ($0 \ll t \ll T/2$) and *backward* ($T/2 \ll t \ll T$) halves of the lattice. In both cases, the t_y integral is dominated by the region in which t_y is close to t , allowing for the propagation of the lightest state over the longest time interval.

In Fig. 3 we show two more diagrams to illustrate two important points concerning our numerical calculation of the correlation functions and of the form factors. The diagram in the left panel shows a *quark-disconnected* contribution to the correlation function originating from the possibility that the external real photon is emitted from sea quarks. In this work we have been using the so-called electroquenched approximation in which the sea-quarks are electrically neutral. In practice this means that we have *neglected* the contributions represented by the diagram in the left panel of Figure 3.

The quark-connected diagram in the right panel of Figure 3 is shown in order to explain the strategy we have used to set the values of the spatial momenta. We exploited the fact that, by working within the electroquenched approximation, i.e. in the absence of the contributions illustrated in the left panel of the figure, it is possible to choose arbitrary values of the spatial momenta by using different spatial boundary conditions for the quark fields [25]. More precisely,

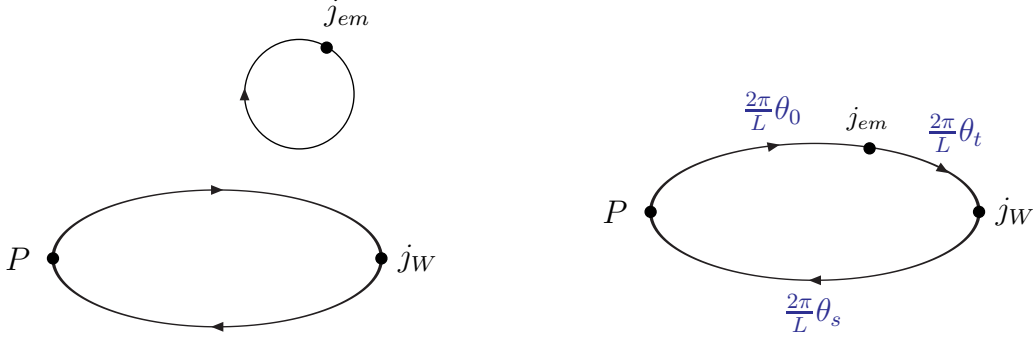


FIG. 3: The diagram on the left represents the contributions to the correlation functions arising from the emission of the photon by the sea quarks. In our numerical simulations we work in the electroquenched approximation and neglect such diagrams. The diagram on the right explains our choice of the spatial boundary conditions, which allow us to set arbitrary values for the meson and photon spatial momenta. The spatial momenta of the valence quarks, modulo $2\pi/L$, in terms of the twisting angles are as indicated. Each diagram implicitly includes all orders in QCD.

we set the boundary conditions for the “spectator” quark such that $\psi(x + \mathbf{n}L) = \exp(2\pi i \mathbf{n} \cdot \boldsymbol{\theta}_s/L) \psi(x)$, where L is the spatial extent of the lattice in each spatial direction. We treat the two propagators that are connected to the electromagnetic current as the results of the Wick contractions of two different fields having the same mass and electric charge but satisfying different boundary conditions [26]. This is possible at the price of accepting tiny violations of unitarity that are exponentially suppressed with the volume. By setting the boundary conditions as illustrated in the figure we have thus been able to choose arbitrary (non-quantised) values for the meson and photon spatial momenta

$$\mathbf{p} = \frac{2\pi}{L} (\boldsymbol{\theta}_0 - \boldsymbol{\theta}_s) , \quad \mathbf{k} = \frac{2\pi}{L} (\boldsymbol{\theta}_0 - \boldsymbol{\theta}_t) , \quad (16)$$

by tuning the real three-vectors $\boldsymbol{\theta}_{0,t,s}$. We find that the most precise results are obtained with small values of $|\mathbf{p}|$ and in particular with $\mathbf{p} = \mathbf{0}$.

The numerical results presented in the following sections have been obtained by setting the non-zero components of the spatial momenta along the third-direction, i.e.

$$\mathbf{p} = (0, 0, |\mathbf{p}|) , \quad \mathbf{k} = (0, 0, E_\gamma) . \quad (17)$$

With this particular choice of the kinematical configuration, a convenient basis for the polarisation vectors of the photon (see Appendix B for more details) is the one in which the *two* physical

polarisation vectors are given by

$$\epsilon_\mu^1 = \left(0, -\frac{1}{\sqrt{2}}, -\frac{1}{\sqrt{2}}, 0\right), \quad \epsilon_\mu^2 = \left(0, \frac{1}{\sqrt{2}}, -\frac{1}{\sqrt{2}}, 0\right), \quad (18)$$

while the unphysical polarisation vectors vanish identically, $\epsilon_\mu^0 = \epsilon_\mu^3 = 0$. Notice that in this basis we have

$$\epsilon^r \cdot p = \epsilon^r \cdot k = 0, \quad (19)$$

and, consequently,

$$H_A^{jr}(k, \mathbf{p}) = \frac{\epsilon_j^r m_P}{2} x_\gamma \left[F_A + \frac{2f_P}{m_P x_\gamma} \right], \quad H_V^{jr}(k, \mathbf{p}) = \frac{i(E_\gamma \epsilon^r \wedge \mathbf{p} - E \epsilon^r \wedge \mathbf{k})^j}{m_P} F_V. \quad (20)$$

Using these formulae, we have built the following numerical estimators

$$R_A(t) = \frac{1}{2m_P} \sum_{r=1,2} \sum_{j=1,2} \frac{R_A^{jr}(t, T/2; \mathbf{k}, \mathbf{p})}{\epsilon_j^r} \rightarrow x_\gamma F_A(x_\gamma) + \frac{2f_P}{m_P}, \quad (21)$$

$$R_V(t) = \frac{m_P}{4} \sum_{r=1,2} \sum_{j=1,2} \frac{R_V^{jr}(t, T/2; \mathbf{k}, \mathbf{p})}{i(E_\gamma \epsilon^r \wedge \mathbf{p} - E \epsilon^r \wedge \mathbf{k})^j} \rightarrow F_V(x_\gamma), \quad (22)$$

for the form factors, which we determine by fitting to the plateaux in the region $0 \ll t \ll T/2$. The discussion here and below corresponds explicitly to the forward half of the lattice ($0 \ll t \ll T/2$). We combine the results with those from the backward half ($T/2 \ll t \ll T$) by exploiting time-reversal symmetry as explained in Appendix B.

The ratios $R_W^{jr}(t, T/2; \mathbf{k}, \mathbf{p})$ appearing in Eqs. (21) and (22), which we evaluate separately for the axial ($W = A$) and vector ($W = V$) components of the weak current, are the finite- T generalisations (see Eq. (B19)) of the ratios $R_W^{\alpha r}(t; \mathbf{k}, \mathbf{p})$ defined above in Eq. (15). The values of the meson energies and of the matrix elements $\langle P|P|0 \rangle$ needed to build these estimators have been obtained from standard effective-mass/residue analyses of pseudoscalar-pseudoscalar two-point functions. We have also computed the pseudoscalar-axial two-point functions from which we have extracted the decay constants f_P on our data sets in order to be able to separate the SD axial form factor F_A from the point-like contribution $2f_P/(m_P x_\gamma)$.

IV. NON-PERTURBATIVE SUBTRACTION OF INFRARED DIVERGENT DISCRETISATION EFFECTS

In this section we want to stress a very important issue associated with infrared divergent cutoff effects which can jeopardise the extraction of F_A at small values of x_γ . We also introduce a strategy to overcome this problem.

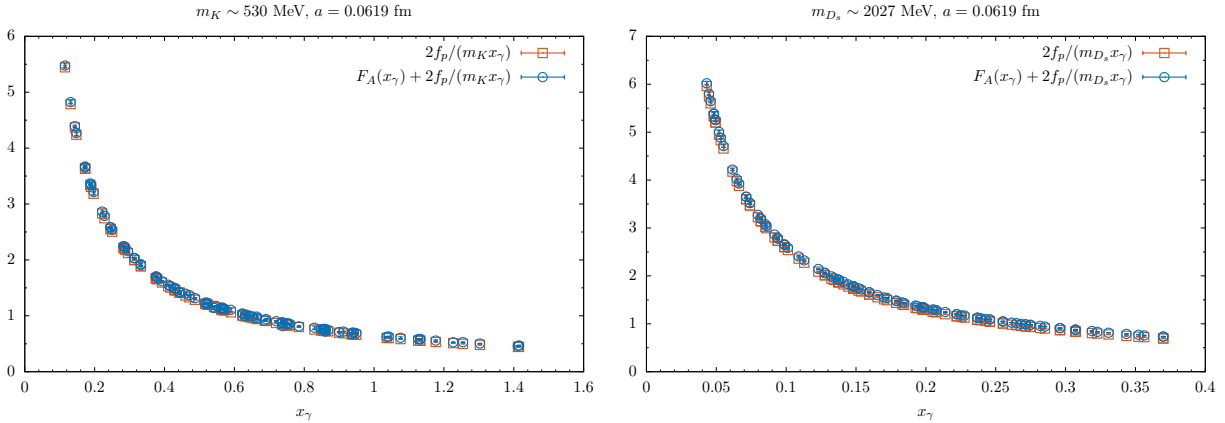


FIG. 4: The blue circles represent $F_A(x_\gamma) + 2f_P/(m_P x_\gamma)$, extracted directly from $R_A(t)$, as a function of x_γ for the K meson (left) and for the D_s meson (right). The red squares represent the point-like contribution given by $2f_P/(m_P x_\gamma)$. The data are taken from the ensemble D15.48 of Ref. [15].

In Fig. 4 we plot $F_A(x_\gamma) + 2f_P/(m_P x_\gamma)$, the sum of the point-like and SD axial form factors which is extracted directly from the correlation functions using $R_A(t)$ (see Eq. (21)), as a function of x_γ for the K (left panel) and the D_s (right panel) mesons. The point-like contribution, $2f_P/(m_P x_\gamma)$, dominates the axial form factor in the full physical range of photon energies and is overwhelming at small x_γ . Using the decay constant and mass, computed in the standard way from the two-point functions, we can in principle subtract the point-like term and extract $F_A(x_\gamma)$. However, this turns out to be very difficult because of the possible presence of discretisation effects which cannot be excluded by the WI of the lattice action. Moreover, these lattice artefacts diverge as $x_\gamma \rightarrow 0$. We now propose a non-perturbative method to eliminate this problem.

At finite lattice spacing the axial form factor is constrained, as in the continuum (see Eq. (4)), by an exact lattice WI

$$\frac{2 \sin(k_\mu a/2)}{a} H_L^{\alpha\mu}(k, \mathbf{p}) = -\langle 0 | j_A^\alpha(0) | P(\mathbf{p}) \rangle = -f_P^L p_L^\alpha, \quad (23)$$

that is true at all orders in the lattice spacing a (see Appendix C). The label L here, and in the remainder of this section, stands for “Lattice” as the discussion concerns the Ward Identity in a discrete space-time. It should not be confused with the spatial extent of the Lattice. This however does not exclude the presence of cutoff effects in Eq. (21). These are terms of $O(a^2)$ ¹ and, in

¹ We assume here that we are using a lattice discretisation in which the leading artefacts are $O(a^2)$. For Wilson Fermions in which they are $O(a)$, the discussion has to be modified accordingly.

particular, include contributions of $O(a^2/x_\gamma)$

$$\frac{R_A(t)}{x_\gamma} \rightarrow \frac{1}{4x_\gamma} \sum_{r=1,2} \sum_{j=1,2} \frac{2H_A^{jr}(k, \mathbf{p})}{\epsilon_j^r m_P} = [F_A(x_\gamma) + a^2 \Delta F_A(x_\gamma)] + \frac{2}{m_P x_\gamma} (f_P + a^2 \Delta f_P) + \dots, \quad (24)$$

where the ellipsis represents higher orders in a^2 , while the quantities ΔF_A and Δf_P depend upon the parameters of the theory regularised on the lattice, on the light and heavy quark masses and upon Λ_{QCD} . Discretisation effects in the pseudoscalar masses are also absorbed into ΔF_A and Δf_P . The crucial point to notice is that the lattice decay constant of the WI in Eq. (23) $f_P^L \neq f_P + a^2 \Delta f_P$. This implies the presence of the extra term of $O(a^2/x_\gamma)$ which appears, in spite of the naive expectations based on the exact lattice WI. Thus the coefficient of the last term in Eq. (24) is not in general given by $2f_P^L/(m_P x_\gamma)$, where f_P^L is the quantity extracted from the axial-pseudoscalar lattice correlation functions at finite lattice spacing. More precisely, once the matrix element $\langle 0|j_A^\alpha(0)|P(p)\rangle$ is parametrised as in Eq. (23), the definition of f_P^L at fixed cut-off depends upon the choice of the index α and of the lattice momentum p_L^α and, for this reason, is not unique. Therefore, given a generic definition of f_P^L , one cannot expect a complete cancellation of the infrared divergent term on the right-hand side of Eq. (24), because a residual lattice artefact will survive

$$F_A^{sub}(x_\gamma) = \frac{1}{4x_\gamma} \sum_{r=1,2} \sum_{j=1,2} \frac{2H_A^{jr}(k, \mathbf{p})}{\epsilon_j^r m_P} - \frac{2f_P^L}{x_\gamma m_P} = F_A(x_\gamma) + a^2 \Delta F_A(x_\gamma) + \frac{2a^2 \Delta \tilde{f}_P}{x_\gamma m_P}, \quad (25)$$

generating an effective, unphysical infrared divergent contribution to $F_A^{sub}(x_\gamma)$ at finite cutoff ($a^2 \Delta \tilde{f}_P = f_P - f_P^L + a^2 \Delta f_P$). This phenomenon is illustrated for the D_s meson in Fig. 5 where F_A^{sub} is plotted as function of x_γ . Since the subtraction of the potentially divergent term is incomplete we observe a fast rise of the effective $F_A^{sub}(x_\gamma)$ at small values of x_γ . For this reason, even if one has data at different values of the lattice spacing, it is particularly difficult to extract the continuum form factor $F_A(x_\gamma)$ from $F_A^{sub}(x_\gamma)$, especially at small x_γ and for heavy mesons. This is illustrated by the intermediate (red) points in Fig. 5 which were obtained by fitting and subtracting the $O(a^2/x_\gamma)$ artefacts. The divergence at small x_γ is reduced but the relative statistical uncertainties are increased.

We now present an alternative strategy that avoids this problem. In Appendix C we show that the correlation function $C_A^{\alpha r}(t; \mathbf{k}, \mathbf{p})$ has a smooth behaviour as a function of \mathbf{k} and that from $C_A^{\alpha r}(t; \mathbf{0}, \mathbf{p})$ it is possible to extract directly $H_A^{ir}(0, \mathbf{p}) = \epsilon_i^r f_P$ (see Eq. (20)). We can then construct

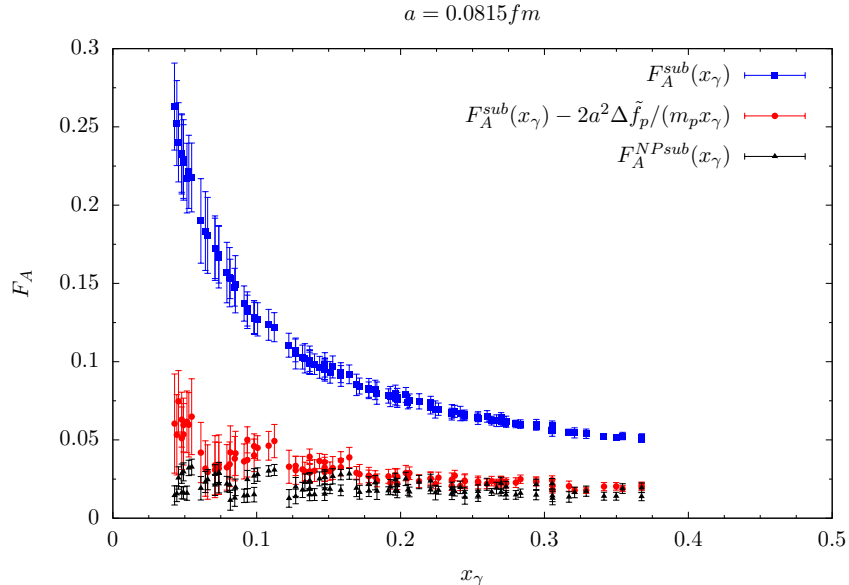


FIG. 5: Study of F_A for the D_s meson. The upper (blue) points show $F_A^{sub}(x_\gamma)$ obtained from Eq. (25). The divergence at small x_γ is reduced by fitting and subtracting the $O(a^2/x_\gamma)$ artefacts, at the price of increased uncertainties at small x_γ ; these are the intermediate (red) points. The most accurate results are given by F_A^{NPsub} , obtained by the non-perturbative subtraction of these artefacts as in Eq. (27) and are shown by the lower (black) points. The data are obtained using the ensemble B55.32 of Ref. [15].

the quantity

$$\bar{R}_A(t) = e^{-tE_\gamma} \frac{\sum_{r=1,2} \sum_{j=1,2} \frac{C_A^{jr}(t, T/2; \mathbf{k}, \mathbf{p})}{\epsilon_j^r}}{\sum_{r=1,2} \sum_{j=1,2} \frac{C_A^{jr}(t, T/2; \mathbf{0}, \mathbf{p})}{\epsilon_j^r}} - 1 \quad (26)$$

that, by construction, vanishes identically at $x_\gamma = 0$. Up to statistical uncertainties, each term in the sums in the numerator and denominator of Eq. (26) is independent of the indices j, r . For the study of the constraints imposed by the electromagnetic Ward identity, it is helpful to view the right-hand side as $H_A^{jr}(k, p)/H_A^{jr}(0, p) - 1$ (which is also independent of j, r). From the improved estimator $\bar{R}_A(t)$ we can extract the structure dependent form factor F_A using

$$\frac{2f_P}{m_P x_\gamma} \bar{R}_A(t) \rightarrow F_A^{NPsub}(x_\gamma) = F_A(x_\gamma) + O(a^2), \quad (27)$$

a quantity that we also show in Fig. 5 and that, in contrast to F_A^{sub} , does not show any divergent behaviour at small x_γ . The reduction of the uncertainty on $F_A(x_\gamma)$ using $\bar{R}_A(t)$, with respect to a fit to the right-hand side of Eq. (25), as shown in Fig. 5, is impressive, particularly at small x_γ and

also for heavy mesons where there are discretisation effects of $O(a^2 m_{D(s)}^2)$. In the following we will only present results obtained with this method.

The knowledge of $C_A^{jr}(t, T/2; \mathbf{0}, \mathbf{p})$ allows us also to define an alternative estimator for the form factor $F_V(x_\gamma)$, namely

$$\bar{R}_V(t) = f_P m_P \frac{\left(\sum_{r=1,2} \sum_{j=1,2} \frac{C_V^{jr}(t, T/2; \mathbf{k}, \mathbf{p}) - C_V^{jr}(t, T/2; \mathbf{0}, \mathbf{p})}{i(E_\gamma \boldsymbol{\epsilon}^r \wedge \mathbf{p} - E \boldsymbol{\epsilon}^r \wedge \mathbf{k})^j} e^{-tE_\gamma} \right)}{\left(\sum_{r=1,2} \sum_{j=1,2} \frac{C_A^{jr}(t, T/2; \mathbf{0}, \mathbf{p})}{\epsilon_j^r} \right)} \rightarrow F_V(x_\gamma), \quad (28)$$

that we find has reduced statistical errors compared to $R_V(t)$. Note that because of parity symmetry the correlation function $C_V^{jr}(t, T/2; \mathbf{0}, \mathbf{p}) = 0$, but this is only approximately true when it is estimated using a finite statistical sample. We find that taking the difference $C_V^{jr}(t, T/2; \mathbf{k}, \mathbf{p}) - C_V^{jr}(t, T/2; \mathbf{0}, \mathbf{p})$ in the numerator of Eq. (28) results in a significant reduction of the statistical uncertainty for physical values of x_γ (see Eq. (7)).

V. NUMERICAL RESULTS

The results presented in this paper were obtained using the ETMC gauge ensembles with $N_f = 2+1+1$ dynamical quarks at three different values of the lattice spacing, $a = 0.0885(36), 0.0815(30)$ and $0.0619(18)$ fm, with meson masses in the range 220-2110 MeV. Details about these ensembles are given in table II of Ref. [15], see also Table I in Appendix D. In total we have included 125 different combinations of momenta obtained by assigning to each of the $\theta_{i=0,t,s}$ five different values; making the same assignments for all choices of the quark masses. In the figures below we illustrate the quality and features of our results by showing examples of plots for light and heavy mesons. The plots used for illustration correspond to unphysical values of the $\overline{\text{MS}}$ renormalised light-quark mass, $m_{ud}(2 \text{ GeV}) = 11.7 \text{ MeV}$. The corresponding meson masses are $m_{D_s} = 2027(3) \text{ MeV}$, $m_D = 1929(6) \text{ MeV}$, $m_K = 530(2) \text{ MeV}$ and $m_\pi = 228(2) \text{ MeV}$. Similar plots can be shown for other values of the simulation parameters.

The scale setting is taken from Ref. [19], where the continuum value of r_0 [27] was obtained imposing $m_\pi^{\text{exp}} = m_{\pi^0} = 134.98 \text{ MeV}$ and $f_\pi^{\text{exp}} = 130.41(20) \text{ MeV}$. The values of the strange and charm quark masses, obtained by extrapolating the kaon and D meson masses to the continuum and at the physical point in the light quark masses, are $m_s(2 \text{ GeV}) = 99.6(4.3) \text{ MeV}$ and $m_c(2 \text{ GeV}) = 1.176(39) \text{ GeV}$. In the following for the renormalised quark mass we shall use $m = \mu/Z_P$, where μ is the twisted mass of the given quark and Z_P is the renormalisation constant of the pseudoscalar density in the $\overline{\text{MS}}$ scheme, at 2 GeV, computed with method M2 [19]. The values of μ used in

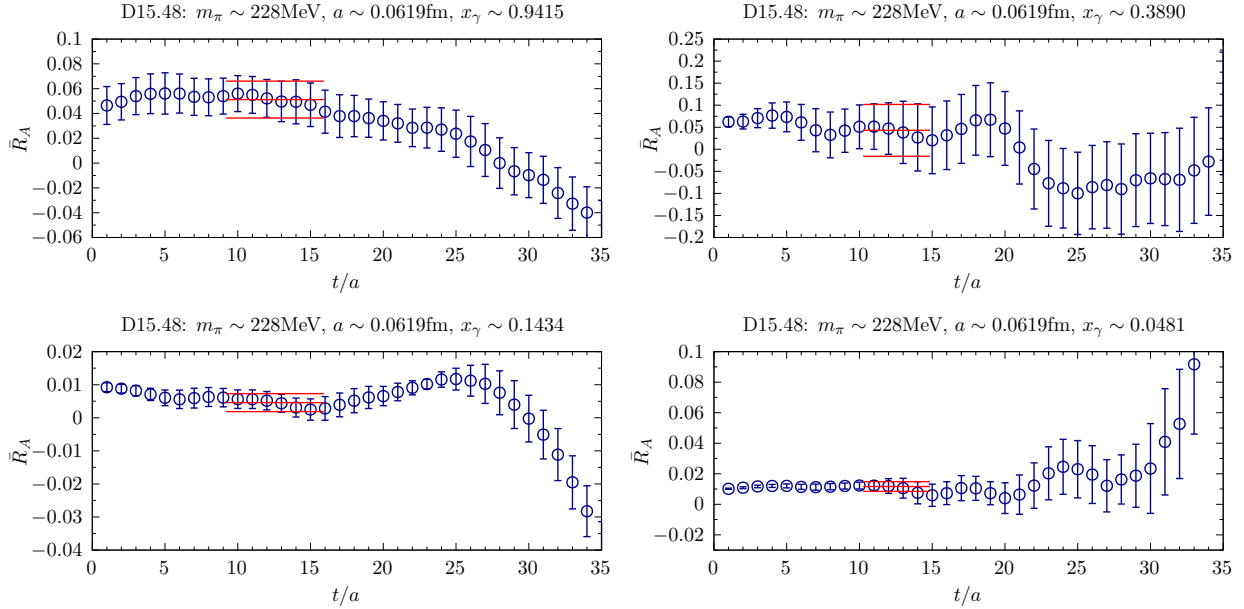


FIG. 6: *Examples of fits to plateaux for the ratio $\bar{R}_A(t)$ for the kaon (left) and D meson (right) at larger (upper panels) or smaller (lower panels) values of x_γ . The values obtained from the fits, together with their uncertainties, are indicated by the horizontal (red) bands.*

our simulation can also be found in Tables I and II in Appendix D (see also Table II of Ref. [15]). Renormalisation of the corresponding axial-vector and vector currents with Twisted Mass Fermions gives $F_A = Z_V F_A^0$ and $F_V = Z_A F_V^0$ where F_A^0 and F_V^0 are the unrenormalised quantities as explained in Eq. (B6), Z_A has been computed with method M2 and Z_V with the WI [19]. In Table II of Appendix D we give further details of our simulation including the values of the angles $\theta_{i=0,s,t}$ used to fix the hadron and photon momenta, see Eq. (17).

In Figs. 6 and 7 we show examples of plateaux for the ratios $\bar{R}_{A,V}(t)$, defined in Eqs. (26) and (28) respectively, for K and D mesons. These figures are representative of the signal quality also for other values of masses, momenta and lattice spacings. The values of all the form factors discussed in the following have been extracted from the plateaux obtained by using Eqs. (26) and (28). The time interval used for the extraction has been chosen, for each of the data ensembles and for each of the mesons, in such a way as to observe a reasonable plateau for all values of the meson/photon momenta. In order to extract the form factors $F_{A,V}$ at physical values of the quark masses and in the continuum limit we have used a variety of fitting formulae for light and heavy mesons as discussed below.

For pions and kaons, we have covered the full physical range of x_γ , $0 \leq x_\gamma \leq 1 - m_\ell^2/m_{\pi,K}^2$

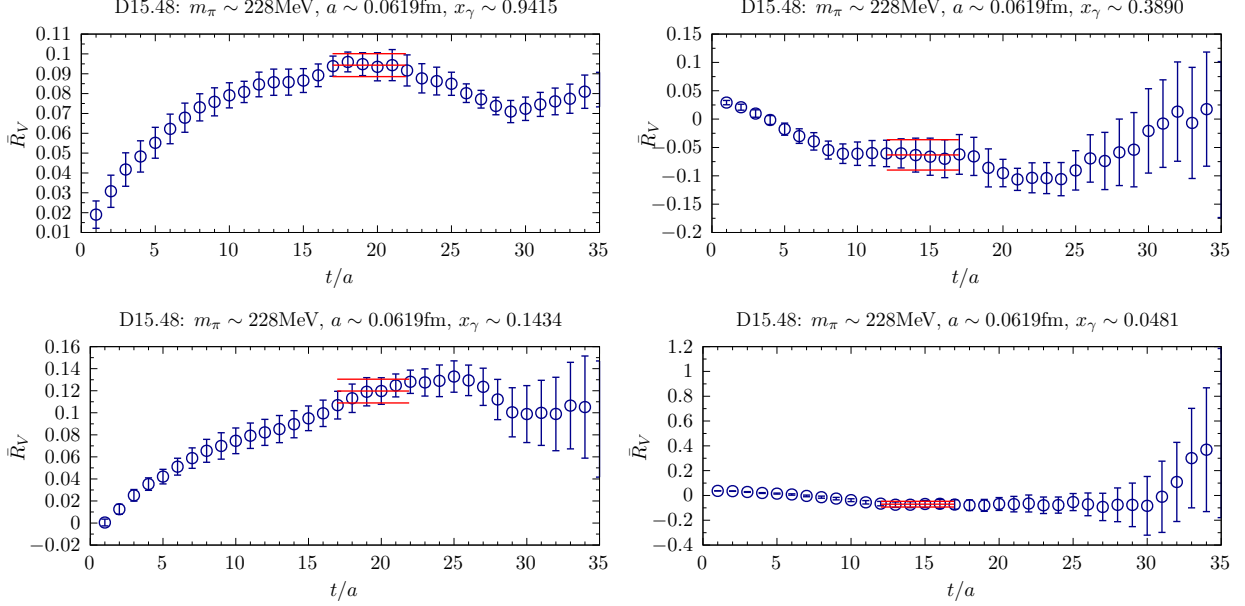


FIG. 7: *Examples of fits to plateaux for the ratio $\bar{R}_V(t)$ for the kaon (left) and D meson (right) at larger (upper panels) or smaller (lower panels) values of x_γ . The values obtained from the fits, together with their uncertainties, are indicated by the horizontal (red) bands.*

(indeed we even have data for unphysical values corresponding to $x_\gamma > 1$).

For the pion, guided by ChPT, we fit to the formula

$$F_{A,V}(x_\gamma) = \frac{m_\pi}{f_\pi} \left[\left(c_0 + c'_0 \frac{m_\pi^2}{(4\pi f_\pi)^2} + \tilde{c}_0 \frac{a^2}{r_0^2} \right) + \left(c'_1 \frac{m_\pi^2}{(4\pi f_\pi)^2} + \tilde{c}_1 \frac{a^2}{r_0^2} \right) x_\gamma \right]. \quad (29)$$

This is certainly not the most general formula to include higher orders terms in ChPT, for example it does not contain chiral logarithms, but it is sufficiently simple and adequate to describe the pion data. The two coefficients \tilde{c}_0 and \tilde{c}_1 take into account possible mass-independent discretisation effects. c'_1 is multiplied by m_π^2 because it arises in higher orders in ChPT. On the other hand the discretisation term proportional to \tilde{c}_1 is not multiplied by the mass of the meson because at this order in a there is an explicit violation of chiral invariance in the lattice Fermion Lagrangian.

When using the simpler expression in Eq. (29) we exclude data at pion masses $m_\pi \gtrsim 350$ MeV. Since in our data we have pion masses up to about 500 MeV, we have also performed fits in the full range by modifying Eq. (29) to include higher order terms as follows:

$$F_{A,V}(x_\gamma) = \frac{m_\pi}{f_\pi} \left[\left(c_0 + c'_0 \frac{m_\pi^2}{(4\pi f_\pi)^2} + \tilde{c}_0 \frac{a^2}{r_0^2} + \Delta c'_0 \frac{m_\pi^4}{(4\pi f_\pi)^4} + \Delta \tilde{c}_0 a^2 m_\pi^2 \right) + \left(c'_1 \frac{m_\pi^2}{(4\pi f_\pi)^2} + \tilde{c}_1 \frac{a^2}{r_0^2} + \Delta c'_1 \frac{m_\pi^4}{(4\pi f_\pi)^4} + \Delta \tilde{c}_1 a^2 m_\pi^2 \right) x_\gamma \right]. \quad (30)$$

The higher-order coefficients $\Delta c'_0$, $\Delta \tilde{c}_0$, \tilde{c}_1 , $\Delta c'_1$ and $\Delta \tilde{c}_1$ have very little effect on the extrapolated results and for this reason they are not well determined. Indeed they only contribute to a slight increase in the uncertainty in the value of the pion form factors at $x_\gamma = 0$ and in the slope in x_γ . Similarly, in the different fits that we performed, we also added some of the possible lattice artefacts that break Lorentz invariance, for example those proportional to $a^2 |\mathbf{k}|^2$ (in the frame where the meson is at rest), where \mathbf{k} is the momentum of the photon. We found that their effect is very small and this was only taken into account in the evaluation of the final uncertainties.

Since $SU(3)$ breaking effects may be important, and we only have results obtained at two values of the *strange* quark mass, for the kaon we first interpolate the form factors to the physical kaon mass and then fit them to the formula

$$F_{A,V}(x_\gamma) = \frac{m_K}{f_K} \left[\left(c_0 + c'_0 \frac{m_\pi^2}{(4\pi f_\pi)^2} + \tilde{c}_0 \frac{a^2}{r_0^2} \right) + \left(c_1 + c'_1 \frac{m_\pi^2}{(4\pi f_\pi)^2} + \tilde{c}_1 \frac{a^2}{r_0^2} \right) x_\gamma \right]. \quad (31)$$

with pion masses $m_\pi < 350$ MeV and

$$F_{A,V}(x_\gamma) = \frac{m_K}{f_K} \left[\left(c_0 + c'_0 \frac{m_\pi^2}{(4\pi f_\pi)^2} + \tilde{c}_0 \frac{a^2}{r_0^2} + \Delta c'_0 \frac{m_\pi^4}{(4\pi f_\pi)^4} + \Delta \tilde{c}_0 a^2 m_\pi^2 \right) + \left(c_1 + c'_1 \frac{m_\pi^2}{(4\pi f_\pi)^2} + \tilde{c}_1 \frac{a^2}{r_0^2} + \Delta c'_1 \frac{m_\pi^4}{(4\pi f_\pi)^4} + \Delta \tilde{c}_1 a^2 m_\pi^2 \right) x_\gamma \right], \quad (32)$$

in the full range of pion masses. Formulae (31) and (32) for the kaon are equivalent to those in (29) and (30) respectively for the pion. The presence of the constant term c_1 in Eqs. (31) and (32) is a reflection of the fact that the strange quark mass is fixed to its physical value. To simplify the notation we have used the same symbols for the coefficients in Eqs. (29)-(32) but the reader should note that their values are different in each case. We do not have sufficient data to include terms proportional to $m_K^2 m_\pi^2$ or m_π^4 with logarithmic corrections in Eq. (32).

In Fig. 8 we present the values of the pion (left panels) and kaon (right panels) form factors $F_A(x_\gamma)$ (upper panels) and $F_V(x_\gamma)$ (lower panels) as a function of x_γ for the configurations at $a = 0.0619$ fm. The plotted points with error bars correspond to different values of the light-quark mass at several values of x_γ . The points with large uncertainties ($\sigma_{F_{A,V}} \geq 0.01$ for the kaon or $\sigma_{F_{A,V}} \geq 0.008$ for the pion) are shown with faint grey symbols. These points are obtained for mesons with substantial non-zero momenta $\mathbf{p} \neq \mathbf{0}$. The results of our simulation are compared to the lowest order in ChPT, given by

$$F_A(x_\gamma) = \text{const.} = \frac{8m_P}{f_P} (L_9^r + L_{10}^r)$$

$$F_V(x_\gamma) = \text{const.} = \frac{m_P}{4\pi^2 f_P}, \quad (33)$$

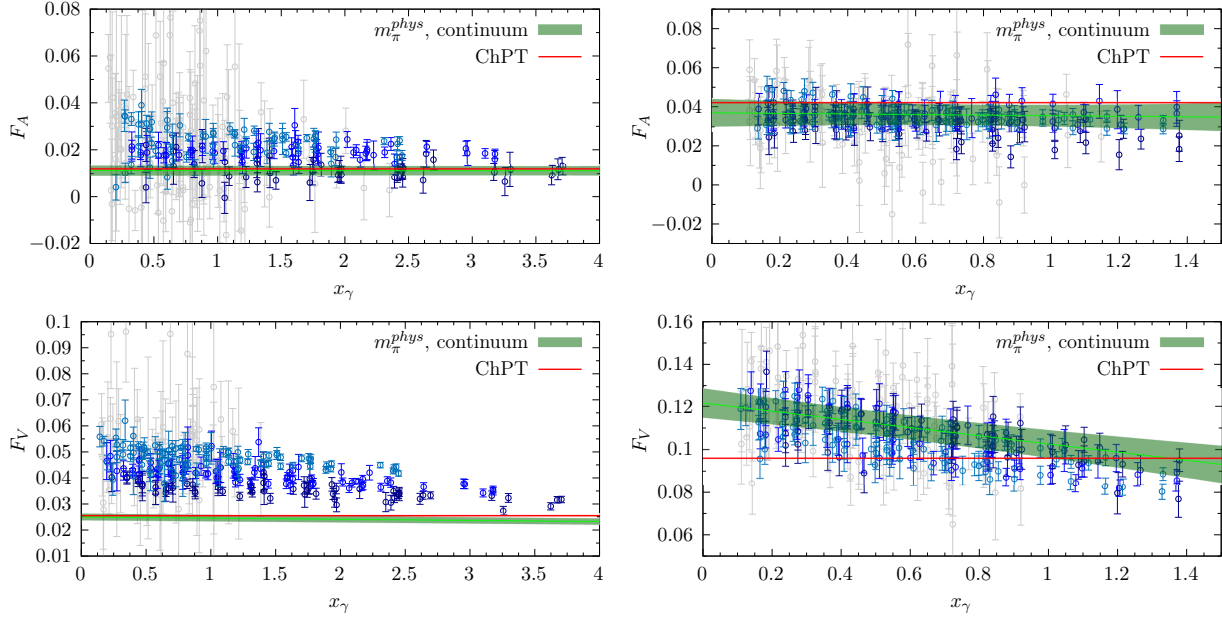


FIG. 8: *Extracted values of the pion (left) and kaon (right) form factors $F_A(x_\gamma)$ (upper) and $F_V(x_\gamma)$ (lower) as a function of x_γ for the configurations at $a = 0.0619$ fm. The horizontal red lines correspond to the lowest order ChPT prediction in Eq.(33). The green lines and bands are the results of the fits, using the formulae given in Eqs. (30) and (32), after extrapolation to the continuum limit and physical quark masses, together with the corresponding uncertainties.*

where P represents π or K and we take $(L_9^r + L_{10}^r) \simeq 0.0017$ [28]; this is indicated by the horizontal red lines. The blue lines and green bands are the results and uncertainties of the fits, obtained using Eqs. (30) and (32) after the extrapolation to physical quark masses and to zero lattice spacing has been performed. In Fig. 9 we show the value of the pion (left) and the kaon (right) form factors $F_A(x_\gamma)$ (upper) and $F_V(x_\gamma)$ (lower) as a function of x_γ , extrapolated to the continuum at the physical point, either using Eqs. (29) and (31) for the pion and kaon respectively to fit the data, full green bands, or by using Eqs. (30) and (32), shaded blue bands. In the figure we also show the values of the form factors for selected values of x_γ extrapolated to the continuum and to the physical point, together with the corresponding statistical and systematic uncertainties. The systematic uncertainties were estimated from the differences in the results coming from different fits of higher order terms in the meson masses, the inclusion of different possible discretisation corrections and the functional forms of the fits, i.e. whether we use Eqs. (29) and (31) for the pion and kaon respectively or Eqs.(30) and (32). The results for the form factors $F_{A,V}$ at selected values of x_γ , the corresponding uncertainties $\Delta_{F_{A,V}}$, and their correlation matrices are given for all the

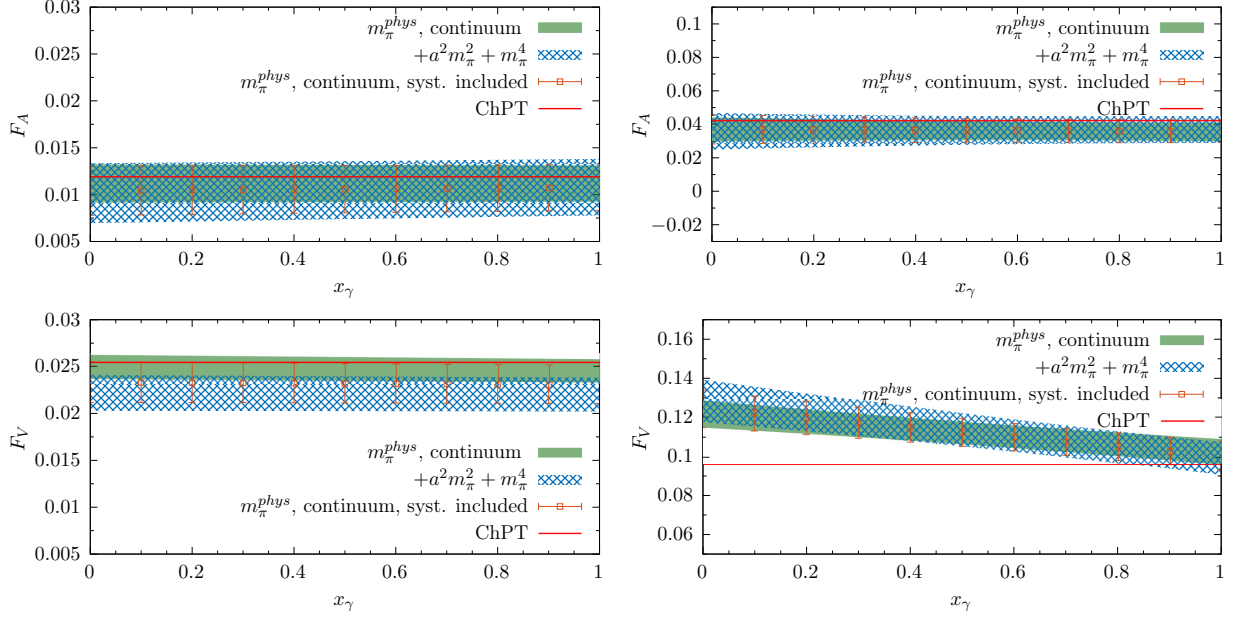


FIG. 9: *Extracted values of the pion (left) and kaon (right) form factors $F_A(x_\gamma)$ (upper) and $F_V(x_\gamma)$ (lower) as a function of x_γ . The horizontal red lines correspond to lowest order ChPT predictions in Eq.(33). The full green bands are the results of the fits after the continuum and chiral extrapolations obtained using Eqs. (29) and (31) for the pion and kaon respectively and the shaded blue bands are obtained using (30) or (32). We also show the extrapolated form factors and the corresponding uncertainties (statistical and systematic) for selected values of x_γ .*

mesons in Appendix D.

For heavy mesons H we expect that the form factors scale as $m_h^{-3/2} \sim f_H/m_H$, where m_h is the mass of the heavy quark contained in H

$$F_{A,V}(x_\gamma) = F_{A,V}^0 \frac{f_H}{m_H} \left(1 + O\left(\frac{\Lambda_{QCD}}{m_H}\right) + \dots \right) + O(a^2 m_H^2), \quad (34)$$

where the constants $F_{A,V}^0$ are a function of the light quark masses. Since, however, for this exploratory study, we have only two values of the heavy quark mass, both around the charm mass, we prefer to interpolate the values of the form factors to the physical charm quark mass and then to fit the result with the simple formula

$$F_{A,V}(x_\gamma) = d_0 + d'_0 \frac{m_\pi^2}{(4\pi f_\pi)^2} + \tilde{d}_0 \frac{a^2}{r_0^2} + \left(d_1 + d'_1 \frac{m_\pi^2}{(4\pi f_\pi)^2} + \tilde{d}_1 \frac{a^2}{r_0^2} \right) x_\gamma. \quad (35)$$

We have also performed fits with the *pole-like* formula

$$F_{A,V}(x_\gamma) = \frac{d_0 + d'_0 \frac{m_\pi^2}{(4\pi f_\pi)^2}}{1 + \left(\Delta_1 + \Delta'_1 \frac{m_\pi^2}{(4\pi f_\pi)^2} \right) x_\gamma} + \tilde{d}_0 \frac{a^2}{r_0^2} + \tilde{d}_1 \frac{a^2}{r_0^2} x_\gamma. \quad (36)$$

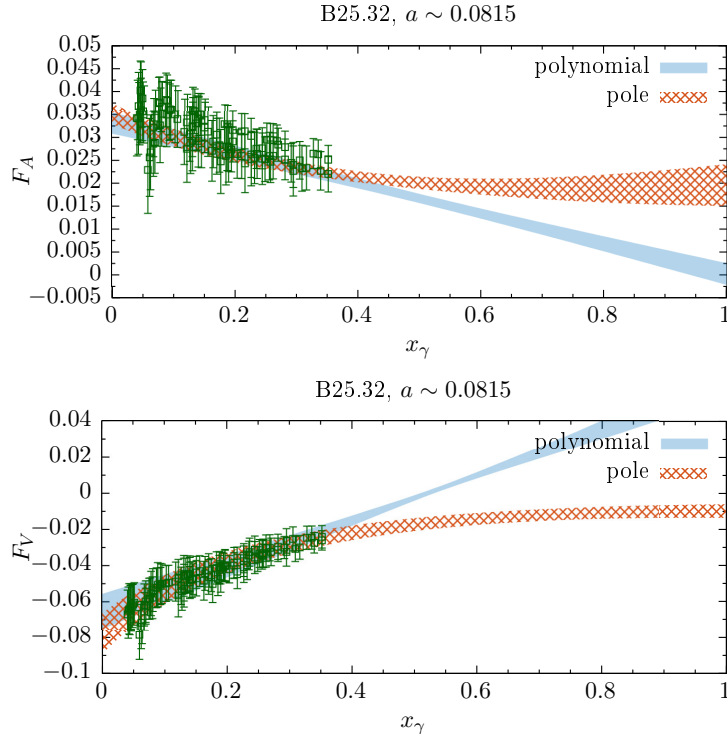


FIG. 10: The form factors $F_A(x_\gamma)$ (upper) and $F_V(x_\gamma)$ (lower) of the D_s meson as a function of x_γ at fixed lattice spacing ($a = 0.0815$ fm) for the ensemble B25.32 [15]. The full blue and shaded orange bands are the results of the fits with the polynomial or pole formulae given in Eqs. (35) and (36) respectively.

In this first study, we only have results for the $D_{(s)}$ mesons in the range $0 \leq x_\gamma \leq 0.4$, corresponding to $E_\gamma \lesssim 400$ MeV in the rest frame of the hadron. In Fig. 10 we give the results for the form factors of the D_s meson, $F_A(x_\gamma)$ and $F_V(x_\gamma)$, at $a = 0.0815$ fm. The full blue and shaded orange bands are the results of the fits with the polynomial or pole formula given in Eqs. (35) and (36) respectively. Since the lattice spacing is fixed, the coefficients $\tilde{d}_{0,1}$ are not included in the fit. We see that the both the fits give a good description of our results in the region where we have data, but differ significantly for $x_\gamma \geq 0.4$. This means that, although both the linear and the pole fits describe accurately the form factors in the region in which we have data, it is not reliable to use these fits in the region $x_\gamma \geq 0.4$. In our future investigations we plan to provide non-perturbative data for the form factors in the full kinematical range $0 \leq x_\gamma \leq 1 - m_\ell^2/m_{D_{(s)}}^2$.

In Fig. 11 we present the values of the form factors $F_A(x_\gamma)$ (upper) and $F_V(x_\gamma)$ (lower) for the D_s meson as a function of x_γ . We show the data obtained at the three different values of the lattice spacing, together with fits using Eq. (35) at each value of the lattice spacing. The orange bands

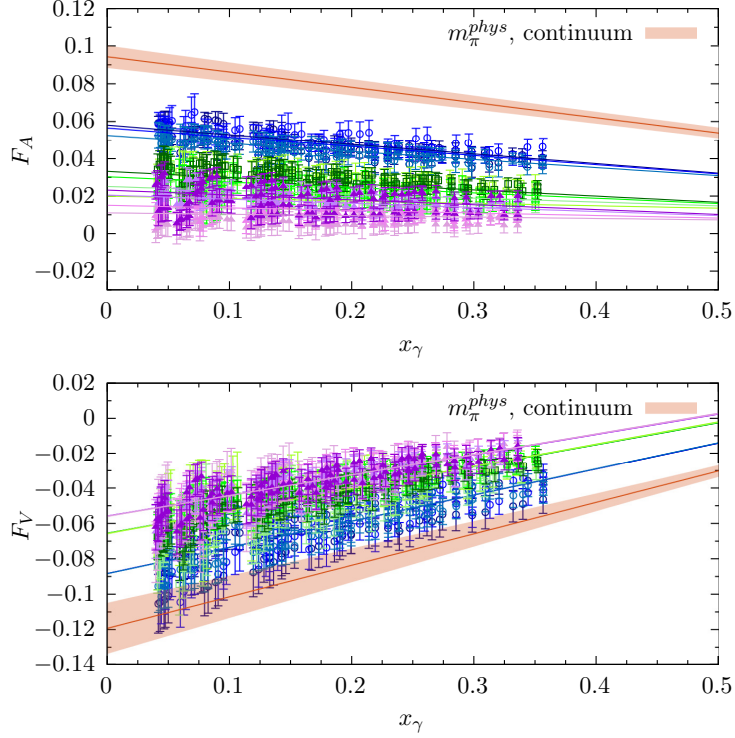


FIG. 11: The form factors $F_A(x_\gamma)$ (upper) and $F_V(x_\gamma)$ (lower) of the D_s meson as a function of x_γ at three values of the lattice spacing with separate fits to the data using Eq. (35) at each value of the lattice spacing. The orange bands with their central red lines represent the result of a single fit to all the data extrapolated to the continuum limit and to physical quark masses.

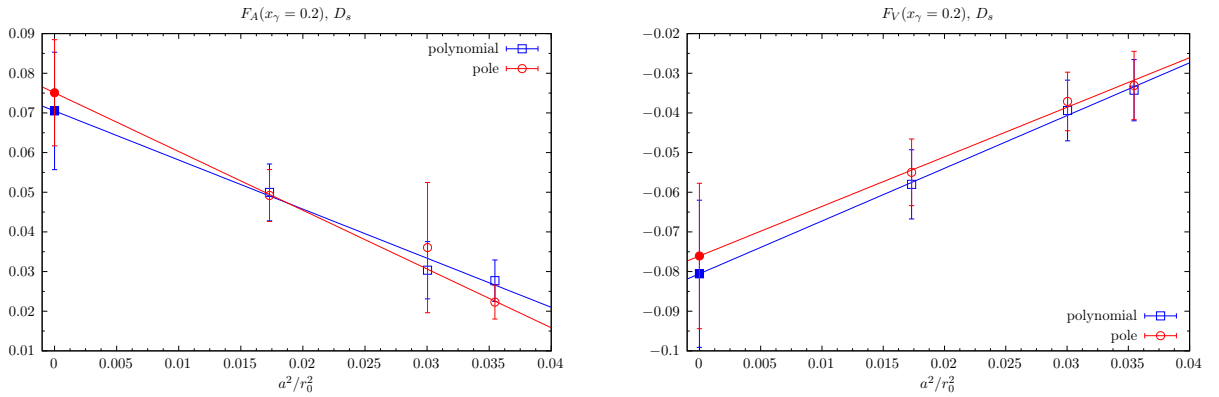


FIG. 12: The form factors F_A (left) and F_V (right) of the D_s meson at $x_\gamma = 0.2$ as functions of a^2 . The polynomial and pole fits correspond to Eqs. (35) and (36) respectively.

with their central red lines are the results of a single fit to all the data after extrapolation to the

continuum limit and to physical quark masses. The discretisation artefacts, which include ones of $O(m_c^2 a^2)$, while approximately of the expected size, appear to be relatively large because the form factors are small. In fact the form factors at the three lattice spacings we have at our disposal are fully consistent, within our uncertainties, with a linear behaviour in a^2 , as illustrated in Fig. 12 where the form factors at $x_\gamma = 0.2$ are presented as a function of the lattice spacing. The points in the figure are obtained after extrapolation to physical quark masses either using a polynomial of pole ansatz corresponding to Eqs. (35) or (36) at fixed lattice spacing. In this first study, with only three lattice spacings at our disposal, we are unable to include corrections of higher order in a^2 beyond those present in Eqs. (35) and (36). In Appendix D we have estimated their effects in the uncertainties of our final results for the form factors.

We also study our physical results (i.e those obtained after the continuum and chiral extrapolations) as a function of x_γ by fitting them to the following linear expressions:

$$F_{A,V}^P(x_\gamma) = C_{A,V}^P + D_{A,V}^P x_\gamma, \quad (37)$$

where P represents each of the pseudoscalar mesons, π , K , D and D_s .

For the axial form factors we find:

$$\begin{aligned} C_A^\pi &= 0.010 \pm 0.003; & D_A^\pi &= 0.0004 \pm 0.0006; & \rho_{C_A^\pi, D_A^\pi} &= -0.419; \\ C_A^K &= 0.037 \pm 0.009; & D_A^K &= -0.001 \pm 0.007; & \rho_{C_A^K, D_A^K} &= -0.673; \\ C_A^D &= 0.109 \pm 0.009; & D_A^D &= -0.10 \pm 0.03; & \rho_{C_A^D, D_A^D} &= -0.557; \\ C_A^{D_s} &= 0.092 \pm 0.006; & D_A^{D_s} &= -0.07 \pm 0.01; & \rho_{C_A^{D_s}, D_A^{D_s}} &= -0.745. \end{aligned} \quad (38)$$

and for the vector form factors we obtain

$$\begin{aligned} C_V^\pi &= 0.023 \pm 0.002; & D_V^\pi &= -0.0003 \pm 0.0003; & \rho_{C_V^\pi, D_V^\pi} &= -0.570; \\ C_V^K &= 0.12 \pm 0.01; & D_V^K &= -0.02 \pm 0.01; & \rho_{C_V^K, D_V^K} &= -0.714; \\ C_V^D &= -0.15 \pm 0.02; & D_V^D &= 0.12 \pm 0.04; & \rho_{C_V^D, D_V^D} &= -0.580; \\ C_V^{D_s} &= -0.12 \pm 0.02; & D_V^{D_s} &= 0.16 \pm 0.03; & \rho_{C_V^{D_s}, D_V^{D_s}} &= -0.900. \end{aligned} \quad (39)$$

In Eqs. (38) and (39), for each of the C 's and D 's, $\rho_{C,D}$ is the correlation between them, defined by

$$\rho_{C,D} = \frac{\sum_i (C_i - \mu_C)(D_i - \mu_D)}{\sqrt{\sum_i (C_i - \mu_C)^2} \sqrt{\sum_i (D_i - \mu_D)^2}}, \quad \mu_C = \frac{1}{N} \sum_i C_i, \quad \mu_D = \frac{1}{N} \sum_i D_i, \quad (40)$$

where C_i and D_i are the jackknife samples and the sum runs over all the jackknives following the procedure in Appendix A of Ref. [29].

For the pion and kaon we can compare the constants $C_{A,V}^{\pi,K}$ in Eqs. (38) and (39) with the constant (i.e. x_γ -independent) values obtained in ChPT using Eq. (33): $F_A^\pi = 0.0119$, $F_V^\pi = 0.0254$, $F_A^K = 0.042$, $F_V^K = 0.096$.

In the remainder of this section we present a brief comparison of our results with experimental data. A more detailed phenomenological analysis will be presented in a separate paper.

For the pion the Particle Data Group (PDG) [1] quotes the following results: $F_A^\pi = 0.0119$ (1) (this value comes from fixing the vector form factor at the CVC prediction from $\pi^0 \rightarrow \gamma\gamma$ decays, $F_V^\pi(x_\gamma = 0) = 1/\alpha\sqrt{2\Gamma(\pi^0 \rightarrow \gamma\gamma)/(\pi m_{\pi^0})} = 0.0259$ (5)) and $F_V^\pi = 0.025$ (2) in nice agreement with our results, respectively $F_A^\pi = C_A^\pi = 0.010$ (3) and $F_V^\pi = C_V^\pi = 0.023$ (2). Also the slope of $F_V^\pi(x_\gamma)$ has been measured from the expression $F_V^\pi(x_\gamma) = F_V^\pi(1)(1 + \lambda(1 - x_\gamma))$ with the result $\lambda = 0.10$ (6), to be compared with our result $\lambda = -D_V^\pi/(C_V^\pi + D_V^\pi) = 0.011$ (12).

For the kaon the PDG quotes the two combinations $F_V^K \pm F_A^K$. They present separate values obtained from $K \rightarrow e$ decays, $F_V^K + F_A^K = 0.133$ (8), and from $K \rightarrow \mu$ decays, $F_V^K + F_A^K = 0.165$ (13). Of course the results should be independent of whether the final-state charged lepton is an electron or muon. For this combination of form factors our value is $F_V^K + F_A^K = 0.161 \pm 0.013$ at $x_\gamma = 0$ and $F_A^K + F_V^K = 0.1363 \pm 0.0096$ at $x_\gamma = 1$. For the other combination of form factors the PDG quotes $F_A^K - F_V^K = -0.21$ (6) obtained from $K \rightarrow \mu$ decays, which is quite different from our result $F_A^K - F_V^K = -0.087 \pm 0.013$ at $x_\gamma = 0$ or $F_A^K - F_V^K = -0.06 \pm 0.01$ at $x_\gamma = 1$. From $K \rightarrow e$ decays there is only the upper bound $F_A^K(0) - F_V^K(0) < 0.49$.

The results in Eqs. (38) and (39) can be combined with the values of the decays constants computed in Ref. [19] and [30]

$$\begin{aligned} f_\pi &= (130.41 \pm 0.20) \text{ MeV} & f_K &= (155.0 \pm 1.9) \text{ MeV} \\ f_D &= (207.4 \pm 3.8) \text{ MeV} & f_{D_s} &= (247.2 \pm 4.1) \text{ MeV}, \end{aligned} \quad (41)$$

to compute the differential or total decay rate using the expressions given in Appendix A.

For completeness, we also present the constants $\tilde{C}_{A,V}^{D(s)}$ and $\tilde{D}_{A,V}^{D(s)}$ which appear in the pole representation of the form factors for D and D_s mesons,

$$F_{A,V}^{D(s)}(x_\gamma) = \frac{\tilde{C}_{A,V}^{D(s)}}{1 + \tilde{D}_{A,V}^{D(s)} x_\gamma} : \quad (42)$$

$$\begin{aligned}
\tilde{C}_A^D &= 0.112 \pm 0.009; & \tilde{D}_A^D &= 1.3 \pm 0.4; & \rho_{\tilde{C}_V^D, \tilde{D}_V^D} &= 0.346; \\
\tilde{C}_V^D &= -0.15 \pm 0.02; & \tilde{D}_V^D &= 1.2 \pm 0.4; & \rho_{\tilde{C}_V^D, \tilde{D}_V^D} &= -0.383;
\end{aligned} \tag{43}$$

$$\begin{aligned}
\tilde{C}_A^{D_s} &= 0.094 \pm 0.006; & \tilde{D}_A^{D_s} &= 1.1 \pm 0.2; & \rho_{\tilde{C}_V^{D_s}, \tilde{D}_V^{D_s}} &= 0.546; \\
\tilde{C}_V^{D_s} &= -0.12 \pm 0.02; & \tilde{D}_V^{D_s} &= 2.6 \pm 0.2; & \rho_{\tilde{C}_V^{D_s}, \tilde{D}_V^{D_s}} &= -0.373.
\end{aligned} \tag{44}$$

CONCLUSIONS

In conclusion we have shown that by using lattice QCD, even with moderate statistics, it is possible to predict with good precision the structure dependent form factors F_A and F_V relevant for $P \rightarrow \ell \bar{\nu}_\ell \gamma$ decays for both light and heavy mesons and that it is also possible to extract their momentum dependence. Previous determinations of these quantities relied either on ChPT for light mesons or on the heavy quark expansion and model-dependent assumptions for heavy mesons. Our work shows that it is possible to compute the relevant form factors from first principles.

We found that the extraction of the axial form factor F_A at small values of x_γ is problematic because of the presence of very large discretisation effects of $O(a^2/(r_0^2 x_\gamma))$ and we provided a procedure for the non-perturbative cancellation of these systematic errors. We also found that for charmed mesons the discretisation effects of $O(a^2 m_H^2)$, while of the expected order of magnitude, are large relative to the small size of the form factors. Nevertheless the results for the form factors at the three lattice spacings are consistent, within our uncertainties, with a linear behaviour in a^2 . Simulations on one or more finer lattices would enable us to improve our estimates of the higher order artefacts and hence reduce the corresponding systematic uncertainty. Such preliminary studies of charmed mesons are also essential in order to study radiative decays of B mesons in the future. In this respect the use of the ratio method may also be very useful [31].

Although the present study clearly can and will be improved by, for example, increasing the statistics, covering the full range of x_γ for D and D_s mesons or simulating on a finer lattice, the results presented in this work already allow for an accurate comparison of the theoretical predictions with experimental measurements and we will discuss the phenomenological implications of our results in a forthcoming paper.

In future we also plan to study the emission of off-shell photons ($k^2 \neq 0$), computing all four form factors appearing in Eq. (3), which would allow us to predict the rates for processes in which the pseudoscalar meson decays into four leptons. These processes are very interesting in the search of physics beyond the Standard Model [32–34].

ACKNOWLEDGMENTS

We gratefully acknowledge helpful discussions with M. Testa. We acknowledge PRACE for awarding us access to Marconi at CINECA, Italy under the grant Pra17-4394. We also acknowledge use of CPU time provided by CINECA under the specific initiative INFN-LQCD123. V.L., G.M. and S.S. thank MIUR (Italy) for partial support under the contract PRIN 2015. C.T.S. was partially supported by STFC (UK) grant ST/P000711/1 and by an Emeritus Fellowship from the Leverhulme Trust. N.T. and R.F. acknowledge the University of Rome Tor Vergata for the support granted to the project PLNUGAMMA. F.S and S.S are supported by the Italian Ministry of Research (MIUR) under grant PRIN 20172LNEEZ. F.S is supported by INFN under GRANT73/CALAT.

Appendix A: Expressions for the decay rates in terms of F_V and F_A

In this appendix we present the explicit formulae needed to evaluate the total and differential decay rates at order α_{em} , combining the non-perturbative determination of the virtual corrections computed with the approach of Ref. [10] with the calculation of the structure-dependent (SD) form factors F_A and F_V determined with the method proposed in this paper. These formulae can be used to compute the double differential decay rates $d^2\Gamma/(dx_\gamma dx_\ell)$, the single differential decay rates, $d\Gamma/dx_\ell$ or $d\Gamma/dx_\gamma$, as well as the integrated decay rate $\Gamma(\Delta E_\gamma) = \int_0^{2\Delta E_\gamma/m_P} dx_\gamma (d\Gamma/dx_\gamma)$ (ΔE_γ is the upper limit on the energy of the emitted photon in the meson rest-frame).

The exchange of a virtual photon depends on the hadron structure, since all momentum modes are included, and the amplitude must therefore be computed non-perturbatively. On the other hand, the non-perturbative evaluation of the amplitude for the emission of a real photon is not strictly necessary [10]. Indeed, it is possible to compute the amplitudes for real-photon emission in perturbation theory when x_γ is sufficiently small that the internal structure of the decaying meson is not resolved. The infrared divergences in the non-perturbatively computed amplitude with the exchange of a virtual photon are cancelled in the decay rates by those present in the emission of a real photon, even when the latter is computed perturbatively. The reason for this cancellation is the universality of the infrared behaviour of the theory (i.e. the infrared divergences do not depend on the structure of the decaying hadron). For large photon energies, for example those present in the decays of heavy mesons, a full non-perturbative determination of the relevant amplitudes is necessary.

To calculate the partial rates for the emission of a hard real photon it is sufficient to know the SD form factors, F_A and F_V , and the meson's decay constant f_P . For the integrated rate $\Gamma(\Delta E_\gamma)$ instead, in the intermediate steps of the calculation it is necessary to introduce an infrared regulator. To this end, in order to work with quantities that are finite when the infrared regulator is removed, it is very useful to organise the inclusive rate $\Gamma(\Delta E_\gamma) = \Gamma(P^- \rightarrow \ell^- \bar{\nu}_\ell(\gamma))|_{E_\gamma \leq \Delta E_\gamma}$ as follows

$$\begin{aligned} \Gamma(\Delta E_\gamma) = \lim_{L \rightarrow \infty} \left[\Gamma_0(L) - \Gamma_0^{\text{pt}}(L) \right] + \lim_{\mu_\gamma \rightarrow 0} \left[\Gamma_0^{\text{pt}}(\mu_\gamma) + \Gamma_1^{\text{pt}}(\Delta E_\gamma, \mu_\gamma) \right] \\ + \left[\Gamma_1(\Delta E_\gamma) - \Gamma_1^{\text{pt}}(\Delta E_\gamma) \right], \end{aligned} \quad (\text{A1})$$

where the subscripts 0, 1 indicate the number of photons in the final state, while the superscript pt denotes the point-like approximation of the decaying meson and μ_γ is an infrared regulator. On the right-hand side of Eq. (A1) the quantities $\Gamma_0(L)$ and $\Gamma_1(\Delta E_\gamma)$ are evaluated on the lattice.

The terms in the first parentheses on the right-hand side of Eq. (A1), $\Gamma_0(L)$ and $\Gamma_0^{\text{pt}}(L)$, have

the same infrared divergences which therefore cancel in the difference. Here we use the lattice size L as the intermediate infrared regulator by working in the QED_L formulation of QED in a finite volume [35] but any other consistent formulation of QED on the lattice can also be used. The difference $\left[\Gamma_0 - \Gamma_0^{\text{pt}}\right]$ is independent of the regulator as this is removed [11]. $\Gamma_0(L)$ depends on the structure of the decaying meson and is computed non-perturbatively Refs. [11–15].

In the terms in the second parentheses on the right-hand side of Eq. (A1) the decaying meson is taken to be a point-like charged particle and both $\Gamma_0^{\text{pt}}(\mu_\gamma)$ and $\Gamma_1^{\text{pt}}(\Delta E_\gamma, \mu_\gamma)$ can be computed directly in infinite volume, in perturbation theory, using some infrared regulator, for example a photon mass $\mu_\gamma = m_\gamma$. Each term is infrared divergent, but the sum is convergent [2] and independent of the infrared regulator. In Refs. [10] and [11] the explicit perturbative calculations of $\left[\Gamma_0^{\text{pt}}(\mu_\gamma) + \Gamma_1^{\text{pt}}(\Delta E_\gamma, \mu_\gamma)\right]$ and $\Gamma_0^{\text{pt}}(L)$ have been performed with a small photon mass μ_γ or using the finite volume respectively, as the infrared regulators.

Finally, the term on second line of the right-hand side of Eq. (A1) is infrared finite. It can be computed in the infinite-volume limit requiring only knowledge of the structure dependent form factors, $F_A(x_\gamma)$ and $F_V(x_\gamma)$ and of the meson's decay constant f_P

$$\left[\Gamma_1(\Delta E_\gamma) - \Gamma_1^{\text{pt}}(\Delta E_\gamma)\right] = \Gamma_{\text{SD}}(\Delta E_\gamma) + \Gamma_{\text{INT}}(\Delta E_\gamma), \quad (\text{A2})$$

where Γ_{SD} is the structure-dependent contribution and Γ_{INT} is that from the interference between the SD and point-like components of the amplitudes. Both Γ_{SD} and Γ_{INT} are separately infrared finite and there is no need to introduce an infrared regulator in this term.

We express the differential decay rate in terms of the following quantities:

- the two dimensionless kinematical variables

$$x_\gamma = \frac{2p \cdot k}{m_P^2}, \quad x_\ell = \frac{2p \cdot p_\ell - m_\ell^2}{m_P^2}, \quad (\text{A3})$$

where m_ℓ the mass of the lepton ℓ , $1 - x_\gamma + x_\gamma r_\ell^2 / (1 - x_\gamma) \leq x_\ell \leq 1$ and $0 \leq x_\gamma \leq 1 - r_\ell^2$, with $r_\ell = m_\ell / m_P$;

- the decay constant of the meson f_P ;
- the two SD axial and vector form factors F_A and F_V .

The differential decay rate is given by the sum of three contributions,

$$\frac{d^2\Gamma}{dx_\gamma dx_\ell} = \frac{\alpha_{em} \Gamma^{(0)}}{4\pi} \left\{ \frac{d^2\Gamma_{\text{pt}}}{dx_\gamma dx_\ell} + \frac{d^2\Gamma_{\text{SD}}}{dx_\gamma dx_\ell} + \frac{d^2\Gamma_{\text{INT}}}{dx_\gamma dx_\ell} \right\}, \quad (\text{A4})$$

where $\Gamma^{(0)}$ is the leptonic decay rate in the absence of electromagnetic corrections. This is given by

$$\Gamma^{(0)} = \frac{G_F^2 |V_{CKM}|^2 f_P^2}{8\pi} m_P^3 r_\ell^2 (1 - r_\ell^2)^2, \quad (\text{A5})$$

where G_F is the Fermi's constant and V_{CKM} the relevant CKM matrix element.

The quantities in the braces on the right-hand side of Eq. (A4) are given by

$$\begin{aligned} \frac{d^2\Gamma_{\text{pt}}}{dx_\gamma dx_\ell} &= \frac{2 f_{\text{pt}}(x_\gamma, x_\ell)}{(1 - r_\ell^2)^2}, \\ \frac{d^2\Gamma_{\text{SD}}}{dx_\gamma dx_\ell} &= \frac{m_P^2 \left\{ [F_V(x_\gamma) + F_A(x_\gamma)]^2 f_{\text{SD}}^+(x_\gamma, x_\ell) + [F_V(x_\gamma) - F_A(x_\gamma)]^2 f_{\text{SD}}^-(x_\gamma, x_\ell) \right\}}{2f_P^2 r_\ell^2 (1 - r_\ell^2)^2}, \\ \frac{d^2\Gamma_{\text{INT}}}{dx_\gamma dx_\ell} &= -\frac{2m_P \left\{ [F_V(x_\gamma) + F_A(x_\gamma)] f_{\text{INT}}^+(x_\gamma, x_\ell) + [F_V(x_\gamma) - F_A(x_\gamma)] f_{\text{INT}}^-(x_\gamma, x_\ell) \right\}}{f_P (1 - r_\ell^2)^2} \end{aligned} \quad (\text{A6})$$

and correspond to the contribution of the point-like approximation, to the SD contribution and to the interference between point-like and SD terms respectively. The kinematical functions appearing in Eq. (A6) are given by

$$\begin{aligned} f_{\text{pt}}(x_\gamma, x_\ell) &= \frac{1 - x_\ell}{x_\gamma^2 (x_\gamma + x_\ell - 1)} \left[x_\gamma^2 + 2(1 - x_\gamma)(1 - r_\ell^2) - \frac{2x_\gamma r_\ell^2 (1 - r_\ell^2)}{x_\gamma + x_\ell - 1} \right], \\ f_{\text{SD}}^+(x_\gamma, x_\ell) &= (x_\gamma + x_\ell - 1) \left[(x_\gamma + x_\ell - 1 + r_\ell^2)(1 - x_\gamma) - r_\ell^2 \right], \\ f_{\text{SD}}^-(x_\gamma, x_\ell) &= -(1 - x_\ell) \left[(x_\ell - 1 + r_\ell^2)(1 - x_\gamma) - r_\ell^2 \right], \\ f_{\text{INT}}^+(x_\gamma, x_\ell) &= -\frac{1 - x_\ell}{x_\gamma (x_\gamma + x_\ell - 1)} \left[(x_\gamma + x_\ell - 1 + r_\ell^2)(1 - x_\gamma) - r_\ell^2 \right], \\ f_{\text{INT}}^-(x_\gamma, x_\ell) &= \frac{1 - x_\ell}{x_\gamma (x_\gamma + x_\ell - 1)} \left[x_\gamma^2 + (x_\gamma + x_\ell - 1 + r_\ell^2)(1 - x_\gamma) - r_\ell^2 \right]. \end{aligned} \quad (\text{A7})$$

The distribution with respect to the photon's momentum is obtained after integrating over the lepton's momentum

$$\frac{d\Gamma}{dx_\gamma} = \int_{x_\ell^{\min}(x_\gamma)}^1 dx_\ell \frac{d^2\Gamma}{dx_\gamma dx_\ell}. \quad (\text{A8})$$

As $x_\gamma \rightarrow 0$ the allowed kinematical range for x_ℓ is squeezed around its maximum, $x_\ell^{\min}(x_\gamma) = 1 - x_\gamma + x_\gamma r_\ell^2 / (1 - x_\gamma) \leq x_\ell \leq 1$. Thus, with the exception of the contribution proportional to

$f_{\text{pt}}(x_\gamma, x_\ell) \sim 1/x_\gamma^2$, all the other contributions vanish in the soft-photon region, which is consequently dominated by the pointlike (eikonal) result

$$\frac{d\Gamma}{dx_\gamma} \sim \int_{x_\ell^{\min}(x_\gamma)}^1 dx_\ell \frac{d^2\Gamma_{\text{pt}}}{dx_\gamma dx_\ell} \sim 1/x_\gamma. \quad (\text{A9})$$

The $1/x_\gamma$ behaviour of the differential rate at small x_γ leads to a logarithmic infrared divergence in the total rate. It is cancelled by the infrared divergence in the $O(\alpha_{em})$ virtual corrections to the inclusive decay rate. The SD and INT contributions vanish at small x_γ .

Eqs. (A4)-(A9) allow us to compute the spectrum $d\Gamma/dx_\gamma$. We advocate organising the determination of the integrated rate in terms of the three sets of parentheses on the right-hand side of Eq. (A1). The procedure to evaluate the term in the first parentheses, $\Gamma_0(L) - \Gamma_0^{\text{pt}}(L)$, is explained in detail in Ref. [10], where the explicit expression for the term in the second parentheses, $\Gamma_0^{\text{pt}}(\mu_\gamma) + \Gamma_1^{\text{pt}}(\Delta E_\gamma, \mu_\gamma)$, can also be found. The third term on the right-hand side of Eq. (A1), $\Gamma_1(\Delta E_\gamma) - \Gamma_1^{\text{pt}}(\Delta E_\gamma) = \Gamma_{\text{SD}} + \Gamma_{\text{INT}}$, is the subject of this paper. As explained above, both Γ_{SD} and Γ_{INT} are infrared finite and are obtained by integrating the differential rates over the physical range of x_γ ,

$$\Gamma_{\text{SD}}(\Delta E_\gamma) = \int_0^{2\Delta E_\gamma/m_P} dx_\gamma \frac{d\Gamma_{\text{SD}}}{dx_\gamma}, \quad \Gamma_{\text{INT}}(\Delta E_\gamma) = \int_0^{2\Delta E_\gamma/m_P} dx_\gamma \frac{d\Gamma_{\text{INT}}}{dx_\gamma}. \quad (\text{A10})$$

Appendix B: Calculating matrix elements from finite Euclidean lattices

In this appendix we derive some useful formulae for the extraction of the two relevant form factors, $F_{A,V}$, from the Euclidean correlation functions expressed in terms of lattice operators on a lattice with finite time extent T .

In order to construct the finite T equivalent of $C_W^{\alpha r}(t; \mathbf{k}, \mathbf{p})$ in Eq.(14), that we will denote as $C_W^{\alpha r}(t, T/2; \mathbf{k}, \mathbf{p})$, it is convenient to define the following hadronic correlation function at fixed t and t_y

$$M_W^{\alpha r}(t_y, t; \mathbf{k}, \mathbf{p}) = \sum_{i=1,2,3} \epsilon_i^r(\mathbf{k}) \sum_{\mathbf{y}} \sum_{\mathbf{x}} e^{-i\mathbf{k}\cdot(\mathbf{y}+\hat{\mathbf{i}}/2)+i\mathbf{p}\cdot\mathbf{x}} \mathbf{T}\langle j_W^\alpha(t) j_{em}^i(t_y, \mathbf{y}) P(0, \mathbf{x}) \rangle_{LT}, \quad (\text{B1})$$

where $\langle \dots \rangle_{LT}$ denotes the average over the gauge field configurations at finite L and T and we introduced suitable independent vectors $\epsilon^r(\mathbf{k})$, $r = 1, 2$, corresponding to the physical polarisations of the emitted photon. A possible simple choice, and one in which the unphysical polarisations

vanish explicitly, is given by

$$\epsilon_\mu^1(\mathbf{k}) \equiv \left(0, \frac{-k_1 k_3}{|\mathbf{k}| \sqrt{k_1^2 + k_2^2}}, \frac{-k_2 k_3}{|\mathbf{k}| \sqrt{k_1^2 + k_2^2}}, \frac{\sqrt{k_1^2 + k_2^2}}{|\mathbf{k}|} \right), \quad \epsilon_\mu^2(\mathbf{k}) \equiv \left(0, \frac{k_2}{\sqrt{k_1^2 + k_2^2}}, -\frac{k_1}{\sqrt{k_1^2 + k_2^2}}, 0 \right). \quad (\text{B2})$$

The polarisation vectors satisfy

$$\sum_{i=1}^3 \epsilon_i^r(\mathbf{k}) k_i = 0, \quad \sum_{i=1}^3 \epsilon_i^r(\mathbf{k}) \epsilon_i^s(\mathbf{k}) = \delta_{rs}. \quad (\text{B3})$$

Since in our simulations we always use $\mathbf{k} = (0, 0, |\mathbf{k}|)$, the polarisation vectors reduce to

$$\epsilon_\mu^1 = \left(0, -\frac{1}{\sqrt{2}}, -\frac{1}{\sqrt{2}}, 0 \right) \quad \epsilon_\mu^2 = \left(0, \frac{1}{\sqrt{2}}, -\frac{1}{\sqrt{2}}, 0 \right). \quad (\text{B4})$$

The ‘‘topology’’ of the correlation function in Eq. (B1) is explained in Figure 2:

- the incoming meson is interpolated at fixed spatial momentum \mathbf{p} by the pseudoscalar operator P placed at time $t = 0$

$$P(0) = \sum_{\mathbf{x}} e^{i\mathbf{p}\cdot\mathbf{x}} P(0, \mathbf{x}); \quad (\text{B5})$$

- the hadronic weak current $j_W^\alpha(t)$ is placed at the generic time t . We used a local discretisation of the weak current that, in the Twisted-Mass discretisation of the fermionic action used in this work [36], is explicitly given by

$$j_W^\alpha(t) = j_V^\alpha(t) - j_A^\alpha(t), \quad j_V^\alpha(t) = Z_A \bar{\psi}_U(t) \gamma^\alpha \psi_D(t), \quad j_A^\alpha(t) = Z_V \bar{\psi}_U(t) \gamma^\alpha \gamma_5 \psi_D(t), \quad (\text{B6})$$

where $j_V^\alpha(t)$ and $j_A^\alpha(t)$ are the vector and axial components that include the corresponding renormalisation factors. Note that the renormalisation factors to be used in Twisted-Mass at maximal twist are chirally-rotated with respect to the ones of standard Wilson fermions [37]. In Eq. (B6) ψ_U indicates the field of an up-type quark that, for the mesons considered in this study, can be either an up or a charm. Similarly, ψ_D can be either a down or a strange quark field. The actions of the up-type and down-type quark fields have been discretised with opposite values of the chirally-rotated Wilson term in order to numerically suppress $O(a^2)$ lattice artefacts in the meson masses [37, 38];

- the electromagnetic current $j_{em}^\mu(t_y, \mathbf{y})$, carrying a three-momentum \mathbf{k} is inserted at $y = (t_y, \mathbf{y})$. This current is defined by

$$j_{em}^\mu(t_y, \mathbf{y}) = \sum_f q_f j_f^\mu(t_y, \mathbf{y}), \quad (\text{B7})$$

where f is the flavour index, q_f is equal to $2/3$ for up-type quarks and to $-1/3$ for down-type quarks. and

$$j_f^\mu(x) = - \left\{ \bar{\psi}_f(x) \frac{\pm i\gamma_5 - \gamma^\mu}{2} U^\mu(x) \psi_f(x + \hat{\mu}) - \bar{\psi}_f(x + \hat{\mu}) \frac{\pm i\gamma_5 + \gamma^\mu}{2} U^\mu(x)^\dagger \psi_f(x) \right\}. \quad (\text{B8})$$

In Eq.(B8) $U_\mu(x)$ are the QCD link variables and the signs \pm are induced by the choice made in the case of the flavour f for the sign of the chirally-rotated Wilson term [17].

We have used $e^{-i\mathbf{k}\cdot(\mathbf{y}+\hat{\mathbf{i}}/2)}$, rather than the simpler, standard exponent $e^{-i\mathbf{k}\cdot\mathbf{y}}$, for the Fourier transform of the current appearing in Eq.(B1)

$$j^r(t_y, \mathbf{k}) = \sum_{i=1}^3 \epsilon_i^r(k) \sum_{\mathbf{y}} e^{-i\mathbf{k}\cdot(\mathbf{y}+\hat{\mathbf{i}}/2)} j_{em}^i(t_y, \mathbf{y}). \quad (\text{B9})$$

Our choice of the exponent, which is equivalent to standard one in the continuum limit, is more convenient for the discussion of the lattice WIs since we have used the point-split exactly conserved electromagnetic current in our simulations.

- A technical subtlety needs to be stressed here. As discussed in the main text, in order to choose arbitrary (non-discretised) values of the spatial momenta for the meson and for the photon, we have introduced a “flavoured” extension of the electromagnetic current (see the explanation in the caption of Figure 3). In practice, in order to have two quarks (ψ_0 and ψ_t , where 0 and t are labels for the quark fields) having the same mass, the same electric charge, the same sign of the chirally-rotated Wilson term but different boundary conditions [26], the expression to be used in the numerical calculation is

$$e^{-i\mathbf{k}\cdot(\mathbf{x}+\hat{\mathbf{i}}/2)} j_f^i(x) = - \left\{ \bar{\chi}_t(x) \frac{\pm i\gamma_5 - \gamma^i}{2} e^{\frac{i\pi(\theta_t^i + \theta_0^i)}{L}} U^i(x) \chi_0(x + \hat{\mathbf{i}}) - \bar{\chi}_t(x + \hat{\mathbf{i}}) \frac{\pm i\gamma_5 + \gamma^i}{2} e^{-\frac{i\pi(\theta_t^i + \theta_0^i)}{L}} U^i(x)^\dagger \chi_0(x) \right\}, \quad (\text{B10})$$

where we have used the fact that (see Eq.(17))

$$\mathbf{k} = \frac{2\pi(\boldsymbol{\theta}_0 - \boldsymbol{\theta}_t)}{L}, \quad \psi_{\{0,t\}}(x + \hat{\mathbf{i}}L) = e^{2\pi i \hat{\mathbf{i}} \cdot \boldsymbol{\theta}_{\{0,t\}}} \psi_{\{0,t\}}(x), \quad (\text{B11})$$

and we have defined, as usually done in implementing twisted boundary conditions [25], the periodic fields

$$\chi_{\{0,t\}}(x) = e^{-\frac{2\pi i \mathbf{x} \cdot \boldsymbol{\theta}_{\{0,t\}}}{L}} \psi_{\{0,t\}}(x). \quad (\text{B12})$$

In all the formulae that will follow the range of the time parameters is extended over the full lattice extension, $0 \leq t < T$ and $0 \leq t_y < T$.

We are now ready to define the finite T correlation function

$$\begin{aligned} C_W^{\alpha r}(t, T/2; \mathbf{k}, \mathbf{p}) = & \\ -i \theta(T/2 - t) \sum_{t_y=0}^T & \left(\theta(T/2 - t_y) e^{E_\gamma t_y} + \theta(t_y - T/2) e^{-E_\gamma(T-t_y)} \right) M_W^{\alpha r}(t_y, t; \mathbf{k}, \mathbf{p}) \\ -i \theta(t - T/2) \sum_{t_y=0}^T & \left(\theta(T/2 - t_y) e^{-E_\gamma t_y} + \theta(t_y - T/2) e^{-E_\gamma(t_y - T)} \right) M_W^{\alpha r}(t_y, t; \mathbf{k}, \mathbf{p}). \end{aligned} \quad (\text{B13})$$

In the continuum and large- T limits one can readily show that for $0 \ll t \ll T/2$

$$C_W^{\alpha r}(t, T/2; \mathbf{k}, \mathbf{p}) \rightarrow C_W^{\alpha r}(t; \mathbf{k}, \mathbf{p}) = H_W^{\alpha r}(k, \mathbf{p}) \frac{e^{-t(E-E_\gamma)} \langle P|P|0 \rangle}{2E} + \dots, \quad (\text{B14})$$

where $C_W^{\alpha r}(t; \mathbf{k}, \mathbf{p})$ is the correlation function introduced in the main text defined in Eq. (14), $H_W^{\alpha r}(k, \mathbf{p})$ is the *physical* matrix element defined in Eq. (1) and the ellipsis represent sub-leading exponentials.

For *negative* time t on the other hand, i.e. for time separations such that $T/2 \ll t \ll T$, in the continuum and large- T limits we have

$$C_W^{\alpha r}(t, T/2; \mathbf{k}, \mathbf{p}) \rightarrow [H_W^{\alpha r}(k, \mathbf{p})]^\dagger \frac{e^{-(T-t)(E-E_\gamma)} \langle 0|P|P \rangle}{2E} + \dots \quad (\text{B15})$$

with the ellipsis again representing the sub-leading exponentials.

It is useful to note that, in order to separate the axial and vector form factors, it is enough to compute separately the correlation functions corresponding to the vector, $C_V^{\alpha r}(t, T/2; \mathbf{k}, \mathbf{p})$, and the axial, $C_A^{\alpha r}(t, T/2; \mathbf{k}, \mathbf{p})$, components of the weak current. Moreover, from the properties

$$[H_A^{\alpha r}(k, \mathbf{p})]^\dagger = H_A^{\alpha r}(k, \mathbf{p}), \quad [H_V^{\alpha r}(k, \mathbf{p})]^\dagger = -H_V^{\alpha r}(k, \mathbf{p}), \quad (\text{B16})$$

we deduce the following properties of the corresponding correlation functions under time reversal:

$$C_A^{\alpha r}(T - t, T/2; \mathbf{k}, \mathbf{p}) = C_A^{\alpha r}(t, T/2; \mathbf{k}, \mathbf{p}), \quad C_V^{\alpha r}(T - t, T/2; \mathbf{k}, \mathbf{p}) = -C_V^{\alpha r}(t, T/2; \mathbf{k}, \mathbf{p}). \quad (\text{B17})$$

Using these relations, the quantities

$$H_A^{ir}(k, \mathbf{p}) = \epsilon_i^r p \cdot k \left[\frac{F_A(p \cdot k)}{m_P} + \frac{f_P}{p \cdot k} \right], \quad H_V^{ir}(k, \mathbf{p}) = i (E_\gamma \boldsymbol{\epsilon}^r \wedge \mathbf{p} - E \boldsymbol{\epsilon}^r \wedge \mathbf{k})^i \frac{F_V(p \cdot k)}{m_P} \quad (\text{B18})$$

were extracted from the ratios of the correlation functions averaged over the two temporal halves of the lattice

$$R_{A,V}^{ir}(t, T/2; \mathbf{k}, \mathbf{p}) = \frac{2 E C_{A,V}^{\alpha r}(t, T/2; \mathbf{k}, \mathbf{p})}{e^{-t(E-E_\gamma)} \langle P|P|0 \rangle} = H_{A,V}^{ir}(k, \mathbf{p}) + \dots \quad (\text{B19})$$

In all the formulae of this Appendix we have used continuum notation for the four vectors but the momentum and energy carried by the current (including the associated projectors) have to be read by performing the following substitutions

$$k^i \rightarrow \hat{k}^i = \frac{2}{a} \sin\left(\frac{ak^i}{2}\right), \quad |\mathbf{k}| \rightarrow |\hat{\mathbf{k}}| = \sqrt{\hat{\mathbf{k}}_1^2 + \hat{\mathbf{k}}_2^2 + \hat{\mathbf{k}}_3^2}, \quad E_\gamma = \frac{2}{a} \sinh^{-1}\left(\frac{a|\hat{\mathbf{k}}|}{2}\right). \quad (\text{B20})$$

In the lattice regularisation that we are using (i.e. Wilson quarks at maximal twist), Eqs. (B16) and (B17) hold for given values of the indices α and $r \in \{1, 2\}$ only up to $O(a^{2n+1})$ lattice artefacts (for integer n). One can show however, that, as a consequence of exact lattice symmetries (see e.g. Refs. [37, 38]) and the choice of momenta and polarisation vectors given in Eqs. (17) and (18), these $O(a^{2n+1})$ cutoff effects cancel if one evaluates appropriate combinations of the relevant correlation functions, namely

$$\frac{1}{4} \sum_{r=1,2} \sum_{j=1,2} C_A^{jr}(t, T/2; \mathbf{k}, \mathbf{p}) / \epsilon_j^r \quad (\text{B21})$$

and

$$\frac{1}{4} \sum_{r=1,2} \sum_{j=1,2} C_V^{jr}(t, T/2; \mathbf{k}, \mathbf{p}) / F_{r,j}(E_\gamma, E), \quad F_{r,j}(E_\gamma, E) = i(E_\gamma \epsilon^r \wedge \mathbf{p} - E \epsilon^r \wedge \mathbf{k})_j, \quad (\text{B22})$$

which are precisely those that occur in Eqs. (26) and (28) of the main text. For the terms in Eqs. (B21) and (B22), the time-reflection properties of Eq. (B17) hold and the derived matrix elements, in addition to satisfying the Hermiticity properties of Eq. (B16), allow for the extraction of the form factors F_A and F_V with no $O(a^{2n+1})$ lattice artefacts. Our analysis of lattice correlators leading to the results in this paper has been based on data obtained from automatically $O(a)$ improved combinations of the form (B21) and (B22).

Appendix C: Exploiting the electromagnetic Ward identity to relate the matrix element $H_A^{\alpha r}(k, \mathbf{p})$ to the decay constant f_P

In this appendix we study the Ward Identity (WI) that relates the axial correlation function $C_A^{\alpha r}(t; \mathbf{k}, \mathbf{p})$ to the axial-pseudoscalar correlation function and, consequently, the matrix element $H_A^{\alpha r}(k, \mathbf{p})$ to the decay constant of the meson f_P . As discussed in the main text, a careful analysis

of the cut-off effects reveals that the WI does not exclude the possibility of different $O(a^2)$ artefacts appearing in the decay constant extracted from the three-point function and that from the two-point function.

We start with a remark about the matrix element of the axial current, determined at a finite lattice spacing a and using a particular lattice discretisation, which we write in the form

$$\langle 0 | j_A^\alpha(0) | P(\mathbf{p}) \rangle = f_P^L p_L^\alpha, \quad (\text{C1})$$

where the combination $f_P^L p_L^\alpha$ is a vector under the orthogonal group $H(4)$ ². At finite a the definition of the lattice decay constant f_P^L depends on the definition that we assume for the lattice momentum p_L^α , for example we may choose $p_L^\alpha = p^\alpha$ or $p_L^\alpha = 2/a \sin[ap^\alpha/2]$, where p^α is the continuum value of the momentum. In particular we define \hat{f}_P by $\langle 0 | j_A^\alpha(0) | P(\mathbf{p}) \rangle = \hat{f}_P(\mathbf{p}) p^\alpha$. Note that $\hat{f}_P = f_P + O(a^2)$, where f_P is the continuum value of the decay constant.

Consider the following correlation function which is relevant to our study,

$$\int d^4y d^3\mathbf{x} e^{-ik \cdot y - i\mathbf{p} \cdot \mathbf{x}} \langle 0 | \text{T} [j_A^\alpha(0) j_{em}^\mu(y) P(-t, -\mathbf{x})] | 0 \rangle. \quad (\text{C2})$$

With Wilson-like Fermions, such as those used in our study, at fixed lattice spacing (for simplicity in the $T \rightarrow \infty$ limit), the electromagnetic WI implies that [39]

$$\begin{aligned} & \frac{1}{a} \sum_{\mu=0}^3 \int d^4y d^3x e^{-ik \cdot y - i\mathbf{p} \cdot \mathbf{x}} \langle 0 | \text{T} [j_A^\alpha(0) \{j_{em}^\mu(y) - j_{em}^\mu(y - \hat{\mu})\} P(-x)] | 0 \rangle \\ &= - \int d^4y d^3x e^{-ik \cdot y - i\mathbf{p} \cdot \mathbf{x}} \{\delta^4(y) - \delta^4(y + x)\} \langle 0 | \text{T} [j_A^\alpha(0) P(-x)] | 0 \rangle, \end{aligned} \quad (\text{C3})$$

where integrals over the spatial coordinates have to be read as lattice sums and, in the case of a real photon, $k^0 = iE_\gamma(\mathbf{k}) = i|\mathbf{k}|$.

The WI can be rewritten in the form

$$\sum_{i=1}^3 \frac{2 \sin(ak_i/2)}{a} C_A^{\alpha i}(t; \mathbf{k}, \mathbf{p}) = C_A^\alpha(t; \mathbf{p}) - C_A^\alpha(t; \mathbf{k}, \mathbf{p}), \quad (\text{C4})$$

where we have defined (note the shift in the exponent with respect to Eq. (C3))

$$C_A^{\alpha\mu}(t; \mathbf{k}, \mathbf{p}) = -i \int d^4y d^3x e^{-ik \cdot (y + \hat{\mu}/2) - i\mathbf{p} \cdot \mathbf{x}} \langle 0 | \text{T} [j_A^\alpha(0) j_{em}^\mu(y) P(-t, -\mathbf{x})] | 0 \rangle, \quad (\text{C5})$$

² In this appendix, as in Sec. IV, the label L stands for ‘‘Lattice’’, as the discussion concerns the Ward Identity in a discrete space-time. It should not be confused here with the spatial extent of the Lattice.

and

$$\begin{aligned}
C_A^\alpha(t; \mathbf{p}) &= \int d^4y d^3x e^{-ik \cdot y - i\mathbf{p} \cdot \mathbf{x}} \delta^4(y) \langle 0 | \text{T} [j_A^\alpha(0) P(-t, -\mathbf{x})] | 0 \rangle \\
&= \int d^3x e^{-i\mathbf{p} \cdot \mathbf{x}} \langle 0 | \text{T} [j_A^\alpha(0) P(-t, -\mathbf{x})] | 0 \rangle \\
C_A^\alpha(t; E_\gamma, \mathbf{p} - \mathbf{k}) &= \int d^4y d^3x e^{-ik \cdot y - i\mathbf{p} \cdot \mathbf{x}} \delta^4(y + x) \langle 0 | \text{T} [j_A^\alpha(0) P(-t, -\mathbf{x})] | 0 \rangle \\
&= \int d^3x e^{E_\gamma t - i(\mathbf{p} - \mathbf{k}) \cdot \mathbf{x}} \langle 0 | \text{T} [j_A^\alpha(0) P(-t, -\mathbf{x})] | 0 \rangle .
\end{aligned} \tag{C6}$$

We can derive the Ward identity for the matrix element itself by going onto the mass shell of the pseudoscalar meson, which in the Euclidean corresponds to selecting the energy of the external hadronic state to be E_P as $|-t|$ becomes very large.

Consider first the case with $\mathbf{k} \neq 0$. In this case the second term on the right-hand side of Eq. (C4) does not contribute because it corresponds to a different energy. Thus, in this case, we have the following identity which is true at all orders in a :

$$\begin{aligned}
\frac{2 \sin(k_\mu a/2)}{a} H_L^{\alpha\mu}(k, \mathbf{p}) &= -i \frac{2 \sin(k_\mu a/2)}{a} \int d^4y e^{-ik \cdot (y + \hat{\mu}/2)} [\langle 0 | \text{T} [j_A^\alpha(0) j_{em}^\mu(y)] | P(\mathbf{p}) \rangle] \\
&= \langle 0 | j_A^\alpha(0) | P(\mathbf{p}) \rangle .
\end{aligned} \tag{C7}$$

Note that to arrive at this identity we do not need to specify the choice of f_P^L . As $a \rightarrow 0$ the discretised derivative in Fourier space $2/a \sin(ak_\mu/2) \rightarrow k_\mu$ and we recover the continuum WI in Eq. (4). We can now proceed in analogy to the continuum and separate $H_L^{\alpha\mu}(k, \mathbf{p})$ into a point-like and a structure-dependent tensor, $H_L^{\alpha\mu}(k, \mathbf{p}) = H_{L-pt}^{\alpha\mu}(k, \mathbf{p}) + H_{L-SD}^{\alpha\mu}(k, \mathbf{p})$ such that

$$\frac{2 \sin(ak_\mu/2)}{a} H_{L-SD}^{\alpha\mu}(k, \mathbf{p}) = 0 \tag{C8}$$

at fixed a . Even in the continuum, the separation of $H^{\alpha\mu}$ into a point-like and a structure-dependent component has an ambiguity in the terms, starting at $O(k^2)$, which are not constrained by the Ward Identity or the equations of motion. Moreover, there are an infinite number of possible point-like lattice-regularised versions of $H_{L-pt}^{\alpha\mu}(k, \mathbf{p})$ which tend to the chosen continuum one as $a \rightarrow 0$.

We choose to define $H_{L-pt}^{\alpha\mu}$ by

$$H_{L-pt}^{\alpha\mu}(k, \mathbf{p}) = f_P^L \left(A(k, \mathbf{p}) \delta^{\alpha\mu} + \frac{T^{\alpha\mu}(k, \mathbf{p})}{\Delta} \right) , \tag{C9}$$

where Δ^{-1} is some version of a lattice boson propagator, for example

$$\Delta^{-1} = \frac{1}{4/a^2 \sum_\rho \sin^2[(p-k)_\rho a/2] + m_P^2} \rightarrow \frac{1}{-2p \cdot k + k^2} + O(a^2) \tag{C10}$$

as $a \rightarrow 0$, $A(k, \mathbf{p}) = 1 + O(a^2)$ and $T^{\alpha\mu}(k, \mathbf{p}) = (2p - k)^\mu (p - k)^\alpha + O(a^2)$ are functions of the momenta which depend on the lattice regularisation and f_P^L is the meson decay constant extracted from the matrix element in Eq. (C1). We therefore have

$$\lim_{a \rightarrow 0} H_{L-pt}^{\alpha\mu}(k, \mathbf{p}) = H_{pt}^{\alpha\mu}(k, \mathbf{p}). \quad (\text{C11})$$

At fixed lattice spacing the only condition that must be satisfied is that in applying the WI,

$$\begin{aligned} \frac{2 \sin(ak_\mu/2)}{a} H_{L-pt}^{\alpha\mu}(k, \mathbf{p}) &= f_P^L \left(\frac{2 \sin(k^\alpha a/2)}{a} A(k, \mathbf{p}) + \frac{2 \sin(k_\mu a/2)}{a} \frac{T^{\alpha\mu}(k, \mathbf{p})}{\Delta} \right) \\ &= f_P^L p_L^\alpha = f_P p^\alpha + O(a^2), \end{aligned} \quad (\text{C12})$$

the denominator Δ of Eq. (C9) disappears. The WI guarantees that the right-hand side of Eq. (C12) is the matrix element $\langle 0 | j_A^\alpha(0) | P(\mathbf{p}) \rangle$ including all orders in a .

By iterating order by order in a , we may find solutions of the form

$$\begin{aligned} A(k, \mathbf{p}) &= 1 + a^2 \tilde{A}(p^2) + O(a^4) \\ T^{\alpha\mu}(k, \mathbf{p}) &= (2p - k)^\mu (p - k)^\alpha + a^2 \tilde{T}^{\alpha\mu}(k, \mathbf{p}) + O(a^4) \end{aligned} \quad (\text{C13})$$

that satisfy the WI, where the coefficients of the expansion are not unique. The only relevant term for the extraction of the form factor F_A however, is the coefficient $A(k, \mathbf{p})$ (since $\epsilon_\mu^r(\mathbf{k}) T^{\alpha\mu}(k, \mathbf{p}) = 0$), which may differ from one by terms of $O(a^2)$ thus giving an *effective* decay constant which is different from the one naively expected from the WI. The absence of lattice artefacts of $O(a^{2n+1})$ is a consequence of our use of the combinations of lattice correlations functions in Eqs. (B21) and (B22) and the resulting $H_L^{\alpha\mu}$ matrix elements (see Eq. (C9)). Alternatively one might work with lattice formulations which preserve chiral symmetry, such as those based on Overlap or Domain Wall fermions. For $O(a)$ improved Wilson fermion lattice actions, instead, corrections of $O(a^3)$ will in general occur.

From the above discussion we conclude that the lattice $H_A^{jr}(k, \mathbf{p})$ has the form

$$H_A^{jr}(k, \mathbf{p}) = \epsilon_j^r \frac{m_P}{2} \left[x_\gamma (F_A(x_\gamma) + a^2 \Delta F_A(x_\gamma)) + \frac{2}{m_P} (f_P + a^2 \Delta f_P) \right] + \dots, \quad (\text{C14})$$

where the dots represent higher order discretisation corrections.

In order to implement the strategy described in Eq. (27), we need to perform a direct calculation of $H_A^{jr}(0, \mathbf{p})$ and hence to study the $k \rightarrow 0$ limit of the WI. The problem is non-trivial because from the spectral analysis of $C_A^{\alpha\mu}(t; \mathbf{k}, \mathbf{p})$ it follows that

$$C_A^{\alpha\mu}(t; \mathbf{k}, \mathbf{p}) = c_1^{\alpha\mu} e^{-tE_P(\mathbf{p})} + c_2^{\alpha\mu} e^{-t\{E_P(\mathbf{p}-\mathbf{k})+E_\gamma(\mathbf{k})\}} + \dots, \quad (\text{C15})$$

where the ellipsis represent exponentially suppressed contributions, with a gap that is $O(m_\pi)$. The first exponential corresponds to the on-shell external meson P and represents the state we are interested in. The second exponential corresponds to the state $P + \gamma$ where both the meson and the photon are on-shell and have a total momentum \mathbf{p} and a relative momentum \mathbf{k} . A similar time dependence also appears in the WI from the rotation of the P source; this is the second term on the right-hand side of Eq. (C4). As discussed above, when $\mathbf{k} \neq 0$ it is possible to isolate the matrix element corresponding to the state P .

The problem we now address is to study the limit $\mathbf{k} \rightarrow \mathbf{0}$, paying special attention to the leading cut-off effects. This can be done by using the exact WI satisfied by $C_A^{\alpha\mu}(t; \mathbf{k}, \mathbf{p})$ at finite lattice spacing; in particular we aim to understand the structure of the correlation function $C_A^{\alpha\mu}(t; \mathbf{k}, \mathbf{p})$ at $\mathbf{k} = 0$. To this end we consider the two-point correlation functions on the right-hand side of Eq. (C4) when α is a spatial index (the case $\alpha = 0$ is similar, but in the following we shall concentrate on the case $\alpha = 1, 2, 3$). By setting $E_\gamma = 0$ in the last term of Eq. (C6), we have

$$C_A^j(t; \mathbf{p}) = \frac{p^j \hat{f}_P(\mathbf{p}) \hat{G}_P(\mathbf{p})}{2\hat{E}_P(\mathbf{p})} e^{-t\hat{E}_P(\mathbf{p})} + \dots, \quad (C15)$$

$$C_A^j(t; E_\gamma = 0, \mathbf{p} - \mathbf{k}) = C_A^j(t, \mathbf{p} - \mathbf{k}) = \frac{(p - k)^j \hat{f}_P(\mathbf{p} - \mathbf{k}) \hat{G}_P(\mathbf{p} - \mathbf{k})}{2\hat{E}_P(\mathbf{p} - \mathbf{k})} e^{-t\hat{E}_P(\mathbf{p} - \mathbf{k})} + \dots, \quad (C16)$$

where the ellipsis represent sub-leading exponentials (the gap is at least $2m_\pi$). In the previous expressions $\hat{f}_P(\mathbf{p}) = f_P + O(a^2)$, $\hat{G}_P(\mathbf{p}) = G_P + O(a^2)$ and $\hat{E}_P(\mathbf{p}) = E_P(\mathbf{p}) + O(a^2)$ where f_P , G_P and $E_P(\mathbf{p})$ are respectively the continuum decay constant, the continuum matrix element of the pseudoscalar density used as interpolating operator, $G_P = \langle 0|P|P(\mathbf{p})\rangle$, and the continuum energy of the meson.

By using the previous two expressions and by differentiating Eq. (C4) with respect to the component k^i of \mathbf{k} and then setting $\mathbf{k} = \mathbf{0}$ we obtain

$$C_A^{ji}(t; \mathbf{0}, \mathbf{p}) = \frac{\hat{f}_P(\mathbf{p}) \hat{G}_P(\mathbf{p})}{2\hat{E}_P(\mathbf{p})} e^{-t\hat{E}_P(\mathbf{p})} \times \left\{ \delta^{ij} + p^j \left[\frac{1}{\hat{f}_P(\mathbf{p})} \frac{\partial \hat{f}_P(\mathbf{p})}{\partial p^i} + \frac{1}{\hat{G}_P(\mathbf{p})} \frac{\partial \hat{G}_P(\mathbf{p})}{\partial p^i} - \left(t + \frac{1}{\hat{E}_P(\mathbf{p})} \right) \frac{\partial \hat{E}_P(\mathbf{p})}{\partial p^i} \right] \right\} + \dots, \quad (C17)$$

where the ellipsis again represents the sub-leading exponentials and we have used the fact that $-\partial_{k_i} g(\mathbf{p} - \mathbf{k}) = \partial_{p_i} g(\mathbf{p} - \mathbf{k})$.

As can be seen, the structure of $C_A^{ji}(t; \mathbf{0}, \mathbf{p})$ is highly non trivial. Note in particular the term linear in t that is a manifestation of the singular behaviour at large distances of the correlation

function (this generates a double pole in momentum space that is at the original the infrared divergence). An important consequence of the strategy proposed in section IV which we have used in our calculations, is that the terms in squared brackets in Eq. (C17) disappear at any value of \mathbf{p} when we contract the correlation function with the physical polarisation vectors of the photon.

With our choice of kinematics, these satisfy the relation

$$\sum_{\mu=0}^3 \epsilon_{\mu}^r(\mathbf{k}) p_{\mu} = \sum_{i=1}^3 \epsilon_i^r(\mathbf{0}) p_i = 0. \quad (\text{C18})$$

Indeed, the $H(3)$ symmetry implies that

$$\frac{\partial \hat{f}_P(\mathbf{p})}{\partial p^i} = p^i \times O(a^2), \quad \frac{\partial \hat{G}_P(\mathbf{p})}{\partial p^i} = p^i \times O(a^2), \quad \frac{\partial \hat{E}_P(\mathbf{p})}{\partial p^i} = \frac{p^i}{E_P(\mathbf{p})} + O(a^2), \quad (\text{C19})$$

and thus

$$C_A^{jr}(t; \mathbf{0}, \mathbf{p}) = \sum_{i=1}^3 \epsilon_i^r(\mathbf{0}) C_A^{ji}(t; \mathbf{0}, \mathbf{p}) = \epsilon_j^r(\mathbf{0}) \frac{\hat{f}_P(\mathbf{p}) \hat{G}_P(\mathbf{p})}{2\hat{E}_P(\mathbf{p})} e^{-t\hat{E}_P(\mathbf{p})} + \dots \quad (\text{C20})$$

We conclude that $C_A^{jr}(t; \mathbf{0}, \mathbf{p})$ can be analyzed as expected to extract the coefficient of the leading exponential. We stress that the above demonstration shows that from $C_A^{jr}(t; \mathbf{0}, \mathbf{p})$ we can extract precisely the decay constant which appears in the lattice matrix element of the axial current in Eq. (C1), without to have to make a choice for the lattice momentum p_L^{α} .

Appendix D

In this Appendix we present some numerical information that may be useful to the reader. We start by listing in Tables I and II the parameters used in our numerical simulations: the values of β and the corresponding lattice spacings, the volumes, the quark mass parameters and the corresponding *pion* masses, m_{π} , and $m_{\pi} L$, the numbers of configurations, and the twisting angles introduced to inject momenta in the correlation functions.

Given the smooth behaviour that we find for the form factors as functions of x_{γ} in the region where we have data, for most phenomenological purposes it is sufficient to use form factors obtained using the ansatz and coefficients given in Section V. However, in the tables in Secs. D 1-D 4 below, we also present the values of the form factors, F_A and F_V at selected values of the photon energy x_{γ} , for the pion, kaon, D and D_s mesons, together with the corresponding uncertainties, Δ_{F_A} and Δ_{F_V} . The results have been extrapolated to the continuum and to physical quark masses. We also give the correlation matrices of these results. For the D and D_s mesons, for which we only have data in a limited range of x_{γ} , the results in Secs. D 3 and D 4 were obtained by averaging

ensemble	β	$a(\text{fm})$	V/a^4	$a\mu_{sea} = a\mu_\ell$	$a\mu_\sigma$	$a\mu_\delta$	N_{cfg}
A30.32	1.90	0.885(18)	$32^3 \times 64$	0.0030	0.15	0.19	150
A40.32				0.0040			100
A60.24	1.90	0.885(18)	$24^4 \times 48$	0.0060	0.15	0.19	150
A80.24				0.0080			150
B25.32	1.95	0.815(30)	$32^3 \times 64$	0.0025	0.135	0.170	150
B35.32				0.0035			150
B55.32				0.0055			150
B75.32				0.0075			80
D15.48	2.10	0.619(18)	$48^3 \times 96$	0.0015	0.12	0.1385	100
D20.48				0.0020			100
D30.48				0.0030			100

TABLE I: Values of the simulated sea and valence quark bare masses for each ensemble used in this work. The table is the same as in Ref. [15] except for μ_s and μ_c which are given in Table II.

the results obtained using Eqs. (37) and (42) and including the difference between the two ansatze in the estimate of the uncertainties. As might be expected from Fig.10 and the accompanying discussion, the extrapolations using the two ansatze diverge significantly at larger x_γ which is reflected in the growing uncertainties in the results in the tables in Secs. D 3 and D 4.

ensemble	β	$L(\text{fm})$	$m_\pi(\text{MeV})$	$m_\pi L$	$a\mu_{\text{sea}} = a\mu_\ell$	$a\mu_s$	$a\mu_c$	$\theta_{i=0,s,t}$		
A30.32	1.90	2.84	273	3.9	0.0030	0.02363,	0.27903,	0, 0.2288, 0.3432,		
A40.32			315	4.5	0.0040			0.02760	0.29900	0.6864, 0.8580
A60.24	1.90	2.13	383	4.1	0.0060					
A80.24			441	4.7	0.0080					
B25.32	1.95	2.61	256	3.4	0.0025	0.02094,	0.24725,	0, 0.2107, 0.3160,		
B35.32			300	4.0	0.0035			0.0239	0.267300	0.6321, 0.7901
B55.32			373	4.9	0.0055					
B75.32			436	6.1	0.0075					
D15.48	2.10	2.97	228	3.4	0.0015	0.01612,	0.19037,	0, 0.2400, 0.3601,		
D20.48			252	3.8	0.0020			0.01910	0.20540	0.7201, 0.9002
D30.48			309	4.7	0.0030					

TABLE II: Central values of the pion mass m_π , of the lattice size L and of the product $m_\pi L$ for the various ensembles used in this work. We also give the values of the angles use to define the z -component of the meson and photon momenta, $\mathbf{p} = (0, 0, \frac{2\pi}{L}(\theta_0 - \theta_s))$ and $\mathbf{k} = (0, 0, \frac{2\pi}{L}(\theta_0 - \theta_t))$ respectively.

1. Results for $F_A(x_\gamma)$ and $F_V(x_\gamma)$ of the pion

F_A Correlation Matrix

x_γ	F_A	Δ_{F_A}
0	0.0104088	0.00262483
0.1	0.0104435	0.00260149
0.2	0.0104782	0.0025792
0.3	0.0105129	0.00255799
0.4	0.0105477	0.00253788
0.5	0.0105824	0.00251889
0.6	0.0106171	0.00250106
0.7	0.0106519	0.00248441
0.8	0.0106866	0.00246897
0.9	0.0107213	0.00245474
1	0.010756	0.00244177

$$\left(\begin{array}{c|c|c|c|c|c|c|c|c|c|c} 1.000 & 1.000 & 0.999 & 0.998 & 0.997 & 0.995 & 0.992 & 0.989 & 0.986 & 0.982 & 0.977 \\ \hline 1.000 & 1.000 & 1.000 & 0.999 & 0.998 & 0.997 & 0.995 & 0.992 & 0.989 & 0.985 & 0.981 \\ \hline 0.999 & 1.000 & 1.000 & 1.000 & 0.999 & 0.998 & 0.996 & 0.994 & 0.992 & 0.989 & 0.985 \\ \hline 0.998 & 0.999 & 1.000 & 1.000 & 1.000 & 0.999 & 0.998 & 0.996 & 0.994 & 0.992 & 0.988 \\ \hline 0.997 & 0.998 & 0.999 & 1.000 & 1.000 & 1.000 & 0.999 & 0.998 & 0.996 & 0.994 & 0.991 \\ \hline 0.995 & 0.997 & 0.998 & 0.999 & 1.000 & 1.000 & 1.000 & 0.999 & 0.998 & 0.996 & 0.994 \\ \hline 0.992 & 0.995 & 0.996 & 0.998 & 0.999 & 1.000 & 1.000 & 1.000 & 0.999 & 0.998 & 0.996 \\ \hline 0.989 & 0.992 & 0.994 & 0.996 & 0.998 & 0.999 & 1.000 & 1.000 & 1.000 & 0.999 & 0.998 \\ \hline 0.986 & 0.989 & 0.992 & 0.994 & 0.996 & 0.998 & 0.999 & 1.000 & 1.000 & 1.000 & 0.999 \\ \hline 0.982 & 0.985 & 0.989 & 0.992 & 0.994 & 0.996 & 0.998 & 0.999 & 1.000 & 1.000 & 1.000 \\ \hline 0.977 & 0.981 & 0.985 & 0.988 & 0.991 & 0.994 & 0.996 & 0.998 & 0.999 & 1.000 & 1.000 \end{array} \right)$$

F_V Correlation Matrix

x_γ	F_V	Δ_{F_V}
0	0.0233352	0.00214581
0.1	0.0233309	0.0021304
0.2	0.0232828	0.00211523
0.3	0.0232566	0.00210031
0.4	0.0232303	0.00208563
0.5	0.0232041	0.00207121
0.6	0.0231779	0.00205705
0.7	0.0231517	0.00204315
0.8	0.0231254	0.00202952
0.9	0.0230992	0.00201617
1	0.023073	0.0020031

$$\left(\begin{array}{c|c|c|c|c|c|c|c|c|c|c} 1.000 & 1.000 & 1.000 & 0.999 & 0.999 & 0.999 & 0.998 & 0.997 & 0.996 & 0.995 & 0.994 \\ \hline 1.000 & 1.000 & 1.000 & 1.000 & 0.999 & 0.999 & 0.998 & 0.998 & 0.997 & 0.996 & 0.995 \\ \hline 1.000 & 1.000 & 1.000 & 1.000 & 1.000 & 0.999 & 0.999 & 0.998 & 0.998 & 0.997 & 0.996 \\ \hline 0.999 & 1.000 & 1.000 & 1.000 & 1.000 & 1.000 & 0.999 & 0.999 & 0.998 & 0.998 & 0.997 \\ \hline 0.999 & 0.999 & 1.000 & 1.000 & 1.000 & 1.000 & 1.000 & 0.999 & 0.999 & 0.998 & 0.998 \\ \hline 0.999 & 0.999 & 0.999 & 1.000 & 1.000 & 1.000 & 1.000 & 1.000 & 0.999 & 0.999 & 0.998 \\ \hline 0.998 & 0.998 & 0.999 & 0.999 & 1.000 & 1.000 & 1.000 & 1.000 & 1.000 & 0.999 & 0.999 \\ \hline 0.997 & 0.998 & 0.998 & 0.999 & 0.999 & 1.000 & 1.000 & 1.000 & 1.000 & 1.000 & 0.999 \\ \hline 0.996 & 0.997 & 0.998 & 0.998 & 0.999 & 0.999 & 1.000 & 1.000 & 1.000 & 1.000 & 1.000 \\ \hline 0.995 & 0.996 & 0.997 & 0.998 & 0.998 & 0.999 & 0.999 & 1.000 & 1.000 & 1.000 & 1.000 \\ \hline 0.994 & 0.995 & 0.996 & 0.997 & 0.998 & 0.998 & 0.999 & 0.999 & 1.000 & 1.000 & 1.000 \end{array} \right)$$

2. Results for $F_A(x_\gamma)$ and $F_V(x_\gamma)$ of the kaon

F_A Correlation Matrix

x_γ	F_A	Δ_{F_A}
0	0.0370382	0.00876335
0.1	0.0369171	0.00828189
0.2	0.0367961	0.00784116
0.3	0.0366751	0.00744839
0.4	0.0365541	0.00711155
0.5	0.0364331	0.00683889
0.6	0.0363121	0.00663833
0.7	0.0361911	0.00651654
0.8	0.0360701	0.00647795
0.9	0.0359491	0.00652404
1	0.035828	0.00665305

$$\begin{pmatrix} 1.000 & 0.998 & 0.990 & 0.975 & 0.951 & 0.916 & 0.869 & 0.808 & 0.736 & 0.654 & 0.566 \\ 0.998 & 1.000 & 0.997 & 0.988 & 0.970 & 0.941 & 0.899 & 0.845 & 0.779 & 0.703 & 0.620 \\ 0.990 & 0.997 & 1.000 & 0.997 & 0.985 & 0.963 & 0.929 & 0.883 & 0.823 & 0.753 & 0.676 \\ 0.975 & 0.988 & 0.997 & 1.000 & 0.996 & 0.982 & 0.957 & 0.918 & 0.867 & 0.805 & 0.734 \\ 0.951 & 0.970 & 0.985 & 0.996 & 1.000 & 0.995 & 0.979 & 0.950 & 0.909 & 0.855 & 0.793 \\ 0.916 & 0.941 & 0.963 & 0.982 & 0.995 & 1.000 & 0.994 & 0.976 & 0.946 & 0.902 & 0.849 \\ 0.869 & 0.899 & 0.929 & 0.957 & 0.979 & 0.994 & 1.000 & 0.994 & 0.975 & 0.943 & 0.900 \\ 0.808 & 0.845 & 0.883 & 0.918 & 0.950 & 0.976 & 0.994 & 1.000 & 0.993 & 0.974 & 0.943 \\ 0.736 & 0.779 & 0.823 & 0.867 & 0.909 & 0.946 & 0.975 & 0.993 & 1.000 & 0.994 & 0.975 \\ 0.654 & 0.703 & 0.753 & 0.805 & 0.855 & 0.902 & 0.943 & 0.974 & 0.994 & 1.000 & 0.994 \\ 0.566 & 0.620 & 0.676 & 0.734 & 0.793 & 0.849 & 0.900 & 0.943 & 0.975 & 0.994 & 1.000 \end{pmatrix}$$

F_V Correlation Matrix

x_γ	F_V	Δ_{F_V}
0	0.12439	0.00960998
0.1	0.121998	0.00891388
0.2	0.119606	0.00828371
0.3	0.117214	0.0077356
0.4	0.114821	0.0072881
0.5	0.112429	0.00696062
0.6	0.110037	0.00677062
0.7	0.107645	0.00672974
0.8	0.105253	0.00684066
0.9	0.102861	0.00709626
1	0.100469	0.00748173

$$\begin{pmatrix} 1.000 & 0.997 & 0.985 & 0.961 & 0.921 & 0.860 & 0.777 & 0.674 & 0.558 & 0.435 & 0.316 \\ 0.997 & 1.000 & 0.996 & 0.980 & 0.949 & 0.898 & 0.825 & 0.731 & 0.622 & 0.506 & 0.391 \\ 0.985 & 0.996 & 1.000 & 0.994 & 0.974 & 0.935 & 0.874 & 0.791 & 0.692 & 0.583 & 0.474 \\ 0.961 & 0.980 & 0.994 & 1.000 & 0.993 & 0.967 & 0.921 & 0.852 & 0.765 & 0.666 & 0.565 \\ 0.921 & 0.949 & 0.974 & 0.993 & 1.000 & 0.991 & 0.961 & 0.909 & 0.837 & 0.752 & 0.661 \\ 0.860 & 0.898 & 0.935 & 0.967 & 0.991 & 1.000 & 0.989 & 0.957 & 0.903 & 0.834 & 0.756 \\ 0.777 & 0.825 & 0.874 & 0.921 & 0.961 & 0.989 & 1.000 & 0.989 & 0.956 & 0.905 & 0.843 \\ 0.674 & 0.731 & 0.791 & 0.852 & 0.909 & 0.957 & 0.989 & 1.000 & 0.989 & 0.958 & 0.914 \\ 0.558 & 0.622 & 0.692 & 0.765 & 0.837 & 0.903 & 0.956 & 0.989 & 1.000 & 0.990 & 0.964 \\ 0.435 & 0.506 & 0.583 & 0.666 & 0.752 & 0.834 & 0.905 & 0.958 & 0.990 & 1.000 & 0.992 \\ 0.316 & 0.391 & 0.474 & 0.565 & 0.661 & 0.756 & 0.843 & 0.914 & 0.964 & 0.992 & 1.000 \end{pmatrix}$$

3. Results for $F_A(x_\gamma)$ and $F_V(x_\gamma)$ of the D meson

x_γ	F_A	Δ_{F_A}
0	0.11029	0.00885428
0.1	0.0988347	0.00740568
0.2	0.0887281	0.00727782
0.3	0.079585	0.00791868
0.4	0.0711547	0.0092365
0.5	0.063267	0.0111973
0.6	0.0558021	0.0137148
0.7	0.0486731	0.0166835
0.8	0.0418154	0.0200096
0.9	0.0351801	0.02362
1	0.0287293	0.027459

F_A Correlation Matrix

1.000	0.907	0.704	0.491	0.314	0.187	0.102	0.049	0.015	-0.006	-0.020
0.907	1.000	0.931	0.776	0.598	0.439	0.314	0.223	0.156	0.108	0.072
0.704	0.931	1.000	0.948	0.827	0.688	0.564	0.465	0.387	0.327	0.281
0.491	0.776	0.948	1.000	0.961	0.875	0.781	0.697	0.627	0.570	0.524
0.314	0.598	0.827	0.961	1.000	0.974	0.921	0.863	0.810	0.764	0.726
0.187	0.439	0.688	0.875	0.974	1.000	0.985	0.954	0.920	0.888	0.859
0.102	0.314	0.564	0.781	0.921	0.985	1.000	0.991	0.974	0.953	0.934
0.049	0.223	0.465	0.697	0.863	0.954	0.991	1.000	0.995	0.985	0.972
0.015	0.156	0.387	0.627	0.810	0.920	0.974	0.995	1.000	0.997	0.991
-0.006	0.108	0.327	0.570	0.764	0.888	0.953	0.985	0.997	1.000	0.998
-0.020	0.072	0.281	0.524	0.726	0.859	0.934	0.972	0.991	0.998	1.000

x_γ	F_V	Δ_{F_V}
0	-0.150466	0.0144033
0.1	-0.135916	0.0119914
0.2	-0.123034	0.0114497
0.3	-0.111365	0.0119456
0.4	-0.100606	0.0132415
0.5	-0.0905481	0.0152892
0.6	-0.0810413	0.0180286
0.7	-0.071976	0.0213636
0.8	-0.0632697	0.0251904
0.9	-0.0548596	0.0294171
1	-0.0466964	0.0339692

F_V Correlation Matrix

1.000	0.925	0.749	0.552	0.377	0.239	0.140	0.072	0.027	-0.003	-0.023
0.925	1.000	0.941	0.807	0.647	0.494	0.364	0.263	0.187	0.130	0.087
0.749	0.941	1.000	0.956	0.851	0.721	0.596	0.488	0.401	0.331	0.276
0.552	0.807	0.956	1.000	0.966	0.885	0.789	0.696	0.615	0.547	0.492
0.377	0.647	0.851	0.966	1.000	0.975	0.918	0.852	0.788	0.732	0.684
0.239	0.494	0.721	0.885	0.975	1.000	0.983	0.946	0.904	0.862	0.824
0.140	0.364	0.596	0.789	0.918	0.983	1.000	0.989	0.966	0.939	0.913
0.072	0.263	0.488	0.696	0.852	0.946	0.989	1.000	0.993	0.979	0.962
0.027	0.187	0.401	0.615	0.788	0.904	0.966	0.993	1.000	0.996	0.987
-0.003	0.130	0.331	0.547	0.732	0.862	0.939	0.979	0.996	1.000	0.997
-0.023	0.087	0.276	0.492	0.684	0.824	0.913	0.962	0.987	0.997	1.000

4. Results for $F_A(x_\gamma)$ and $F_V(x_\gamma)$ of the D_s meson

F_A Correlation Matrix

x_γ	F_A	Δ_{F_A}
0	0.09307	0.00598514
0.1	0.0849608	0.00486963
0.2	0.0776688	0.00422644
0.3	0.0709899	0.00389515
0.4	0.0647833	0.00400167
0.5	0.0589483	0.00469896
0.6	0.0534115	0.00595597
0.7	0.0481175	0.00763605
0.8	0.0430239	0.00962076
0.9	0.0380979	0.0118319
1	0.0333133	0.0142191

1.000	0.959	0.862	0.725	0.537	0.338	0.186	0.091	0.034	0.001	-0.020
0.959	1.000	0.966	0.861	0.664	0.423	0.224	0.091	0.006	-0.048	-0.084
0.862	0.966	1.000	0.957	0.802	0.569	0.357	0.206	0.105	0.037	-0.010
0.725	0.861	0.957	1.000	0.937	0.768	0.583	0.437	0.334	0.261	0.208
0.537	0.664	0.802	0.937	1.000	0.942	0.824	0.713	0.626	0.561	0.512
0.338	0.423	0.569	0.768	0.942	1.000	0.966	0.906	0.848	0.802	0.764
0.186	0.224	0.357	0.583	0.824	0.966	1.000	0.984	0.956	0.928	0.903
0.091	0.091	0.206	0.437	0.713	0.906	0.984	1.000	0.993	0.979	0.965
0.034	0.006	0.105	0.334	0.626	0.848	0.956	0.993	1.000	0.996	0.989
0.001	-0.048	0.037	0.261	0.561	0.802	0.928	0.979	0.996	1.000	0.998
-0.020	-0.084	-0.010	0.208	0.512	0.764	0.903	0.965	0.989	0.998	1.000

F_V Correlation Matrix

x_γ	F_V	Δ_{F_V}
0	-0.120018	0.0155225
0.1	-0.0989568	0.0117214
0.2	-0.0824261	0.00951697
0.3	-0.0684115	0.00783577
0.4	-0.05594	0.00806476
0.5	-0.0444834	0.0110619
0.6	-0.03373	0.0158477
0.7	-0.0234841	0.0215682
0.8	-0.0136163	0.0278383
0.9	-0.00403801	0.0344741
1	0.00531392	0.0413737

1.000	0.933	0.886	0.898	0.782	0.543	0.379	0.288	0.236	0.205	0.184
0.933	1.000	0.989	0.935	0.667	0.317	0.107	-0.004	-0.066	-0.103	-0.127
0.886	0.989	1.000	0.955	0.679	0.314	0.093	-0.024	-0.090	-0.130	-0.157
0.898	0.935	0.955	1.000	0.862	0.571	0.369	0.255	0.188	0.147	0.119
0.782	0.667	0.679	0.862	1.000	0.908	0.787	0.707	0.656	0.623	0.600
0.543	0.317	0.314	0.571	0.908	1.000	0.973	0.938	0.912	0.893	0.879
0.379	0.107	0.093	0.369	0.787	0.973	1.000	0.993	0.982	0.972	0.965
0.288	-0.004	-0.024	0.255	0.707	0.938	0.993	1.000	0.998	0.993	0.990
0.236	-0.066	-0.090	0.188	0.656	0.912	0.982	0.998	1.000	0.999	0.997
0.205	-0.103	-0.130	0.147	0.623	0.893	0.972	0.993	0.999	1.000	1.000
0.184	-0.127	-0.157	0.119	0.600	0.879	0.965	0.990	0.997	1.000	1.000

-
- [1] M. Tanabashi *et al.* [Particle Data Group], Phys. Rev. D **98** (2018) no.3, 030001. doi:10.1103/PhysRevD.98.030001;
<http://pdg.lbl.gov/2018/reviews/rpp2018-rev-form-factors-radiative-pik-decays.pdf>;
<http://pdg.lbl.gov/2018/reviews/rpp2018-rev-pseudoscalar-meson-decay-cons.pdf>
- [2] F. Bloch and A. Nordsieck, Phys. Rev. **52** (1937) 54. doi:10.1103/PhysRev.52.54
- [3] S. Weinberg, “The Quantum theory of fields. Vol. 1: Foundations,”
- [4] F. E. Low, Phys. Rev. **96** (1954) 1428. doi:10.1103/PhysRev.96.1428
- [5] J. Bijnens and P. Talavera, Nucl. Phys. B **489** (1997) 387 doi:10.1016/S0550-3213(97)00069-2 [hep-ph/9610269].
- [6] C. Q. Geng, I. L. Ho and T. H. Wu, Nucl. Phys. B **684** (2004) 281 doi:10.1016/j.nuclphysb.2003.12.039 [hep-ph/0306165].
- [7] V. Mateu and J. Portoles, Eur. Phys. J. C **52** (2007) 325 doi:10.1140/epjc/s10052-007-0393-5 [arXiv:0706.1039 [hep-ph]].
- [8] R. Unterdorfer and H. Pichl, Eur. Phys. J. C **55** (2008) 273 doi:10.1140/epjc/s10052-008-0584-8 [arXiv:0801.2482 [hep-ph]].
- [9] V. Cirigliano, G. Ecker, H. Neufeld, A. Pich and J. Portoles, Rev. Mod. Phys. **84** (2012) 399 doi:10.1103/RevModPhys.84.399 [arXiv:1107.6001 [hep-ph]].
- [10] N. Carrasco, V. Lubicz, G. Martinelli, C. T. Sachrajda, N. Tantalo, C. Tarantino and M. Testa, Phys. Rev. D **91** (2015) no.7, 074506 doi:10.1103/PhysRevD.91.074506 [arXiv:1502.00257 [hep-lat]].
- [11] V. Lubicz, G. Martinelli, C. T. Sachrajda, F. Sanfilippo, S. Simula and N. Tantalo, Phys. Rev. D **95** (2017) no.3, 034504 doi:10.1103/PhysRevD.95.034504 [arXiv:1611.08497 [hep-lat]].
- [12] V. Lubicz, G. Martinelli, C. T. Sachrajda, F. Sanfilippo, S. Simula, N. Tantalo and C. Tarantino, PoS LATTICE **2016** (2016) 290 doi:10.22323/1.256.0290 [arXiv:1610.09668 [hep-lat]].
- [13] N. Tantalo, V. Lubicz, G. Martinelli, C. T. Sachrajda, F. Sanfilippo and S. Simula, arXiv:1612.00199 [hep-lat].
- [14] D. Giusti, V. Lubicz, G. Martinelli, C. T. Sachrajda, F. Sanfilippo, S. Simula, N. Tantalo and C. Tarantino, Phys. Rev. Lett. **120** (2018) no.7, 072001 doi:10.1103/PhysRevLett.120.072001 [arXiv:1711.06537 [hep-lat]].
- [15] M. Di Carlo *et al.*, Phys. Rev. D **100** (2019) no.3, 034514 [arXiv:1904.08731 [hep-lat]]
- [16] G. M. de Divitiis *et al.*, JHEP **1204** (2012) 124 doi:10.1007/JHEP04(2012)124 [arXiv:1110.6294 [hep-lat]].
- [17] G. M. de Divitiis *et al.* [RM123 Collaboration], Phys. Rev. D **87** (2013) no.11, 114505 doi:10.1103/PhysRevD.87.114505 [arXiv:1303.4896 [hep-lat]].
- [18] D. Becirevic, B. Haas and E. Kou, Phys. Lett. B **681** (2009) 257 doi:10.1016/j.physletb.2009.10.017 [arXiv:0907.1845 [hep-ph]].

- [19] N. Carrasco *et al.* [European Twisted Mass Collaboration], Nucl. Phys. B **887**, 19 (2014) doi:10.1016/j.nuclphysb.2014.07.025 [arXiv:1403.4504 [hep-lat]].
- [20] G. M. de Divitiis *et al.*, arXiv:1908.10160 [hep-lat].
- [21] C. Kane, C. Lehner, S. Meinel and A. Soni, arXiv:1907.00279 [hep-lat].
- [22] J. Bijnens, G. Ecker and J. Gasser, Nucl. Phys. B **396** (1993) 81 [hep-ph/9209261].
- [23] M. Beneke, V. M. Braun, Y. Ji and Y. B. Wei, JHEP **1807** (2018) 154 doi:10.1007/JHEP07(2018)154 [arXiv:1804.04962 [hep-ph]].
- [24] L. Maiani and M. Testa, Phys. Lett. B **245** (1990) 585. doi:10.1016/0370-2693(90)90695-3
- [25] G. M. de Divitiis, R. Petronzio and N. Tantalo, Phys. Lett. B **595** (2004) 408 doi:10.1016/j.physletb.2004.06.035 [hep-lat/0405002].
- [26] J. M. Flynn, A. Juttner, C. T. Sachrajda, P. A. Boyle and J. M. Zanotti, JHEP **0705** (2007) 016 doi:10.1088/1126-6708/2007/05/016 [hep-lat/0703005 [HEP-LAT]].
- [27] R. Sommer, Nucl. Phys. B **411** (1994) 839 doi:10.1016/0550-3213(94)90473-1 [hep-lat/9310022].
- [28] J. Bijnens and G. Ecker, Ann. Rev. Nucl. Part. Sci. **64** (2014) 149 [arXiv:1405.6488 [hep-ph]].
- [29] L. Del Debbio, L. Giusti, M. Lüscher, R. Petronzio, and N. Tantalo, JHEP **02** (2007) 082, [hep-lat/0701009].
- [30] N. Carrasco *et al.*, Phys. Rev. D **91**, no. 5, 054507 (2015) doi:10.1103/PhysRevD.91.054507 [arXiv:1411.7908 [hep-lat]].
- [31] B. Blossier *et al.* [ETM Collaboration], JHEP **1004** (2010) 049 doi:10.1007/JHEP04(2010)049 [arXiv:0909.3187 [hep-lat]].
- [32] V. Barger, C. W. Chiang, W. Y. Keung and D. Marfatia, Phys. Rev. Lett. **108** (2012) 081802 doi:10.1103/PhysRevLett.108.081802 [arXiv:1109.6652 [hep-ph]].
- [33] B. Batell, D. McKeen and M. Pospelov, Phys. Rev. Lett. **107** (2011) 011803 doi:10.1103/PhysRevLett.107.011803 [arXiv:1103.0721 [hep-ph]].
- [34] J. Albrecht, E. Stamou, R. Ziegler and R. Zwicky, arXiv:1911.05018 [hep-ph].
- [35] M. Hayakawa and S. Uno, Prog. Theor. Phys. **120** (2008) 413 [arXiv:0804.2044 [hep-ph]].
- [36] R. Frezzotti *et al.* [Alpha Collaboration], JHEP **0108** (2001) 058 [hep-lat/0101001].
- [37] R. Frezzotti and G. C. Rossi, JHEP **0408** (2004) 007 doi:10.1088/1126-6708/2004/08/007 [hep-lat/0306014].
- [38] R. Frezzotti and G. C. Rossi, JHEP **0410** (2004) 070 doi:10.1088/1126-6708/2004/10/070 [hep-lat/0407002].
- [39] M. Bochicchio, L. Maiani, G. Martinelli, G. C. Rossi and M. Testa, Nucl. Phys. B **262** (1985) 331. doi:10.1016/0550-3213(85)90290-1